## Title

# Illuminating microbial mat assembly: Cyanobacteria and Chloroflexota cooperate to structure light-responsive biofilms


## Authors

Freddy Bunbury[1,2,*], Carlos Rivas[2], Victoria Calatrava[2], Andrey Malkovskiy[2], Lydia-Marie Joubert[3], Amar D. Parvate[4], James E. Evans[4,5], Arthur Grossman[2,6], Devaki Bhaya[2,6,*]

## Affiliations

1. Department of Ecology and Evolution, The University of Chicago, Chicago, IL 60637, USA
2. Department of Plant Biology, Carnegie Institution for Science, 260 Panama St., Stanford, CA 94305, USA
3. SLAC National Accelerator Laboratory, Division of CryoEM and Bioimaging, Menlo Park, CA 94025, USA
4. Pacific Northwest National Laboratory, Environmental Molecular Sciences Laboratory, Richland, WA, USA
5. Washington State University Pullman, School of Biological Sciences, Pullman, WA, USA
6. Stanford University, Biology Department, Stanford, CA 94305, USA

*Corresponding authors: Freddy Bunbury (freddy.bunbury@gmail.com), Devaki Bhaya (dbhaya@carnegiescience.edu)



## Abstract

Microbial mats are stratified communities often dominated by unicellular and filamentous phototrophs within an exopolymer matrix. It is challenging to quantify the dynamic responses of community members *in situ* as they experience steep gradients and rapid fluctuations of light. To address this, we developed a binary consortium using two representative isolates from hot spring mats, the unicellular oxygenic phototrophic cyanobacterium *Synechococcus* OS-B' (Syn OS-B') and the filamentous anoxygenic phototroph *Chloroflexus* MS-CIW-1 (Chfl MS-1). We quantified the motility of individual cells and entire colonies and demonstrated that Chfl MS-1 formed bundles of filaments that moved in all directions with no directional bias to light. Syn OS-B' was slightly less motile but exhibited positive phototaxis. This binary consortium displayed cooperative behavior by moving further than either species alone and formed ordered arrays where both species aligned with the light source. No cooperative motility was observed when a non-motile *pilB* mutant of Syn OS-B' was used instead of Syn OS-B'. The binary consortium also produced more adherent biofilm than individual species, consistent with the close interspecies association revealed by electron microscopy. We propose that cyanobacteria and Chloroflexota cooperate in forming natural microbial mats, by colonizing new niches and building robust biofilms.

## Introduction

Stratified microbial mats dominated by phototrophs are examples of complex biofilms that often thrive in extreme environments such as hot springs, desert crusts, and hypersaline lagoons (1). These dense biofilms experience light fluctuations due to changing cloud cover and more predictable diel oscillations: increasing sunlight in the morning drives oxygenic photosynthesis, which increases $O_2$ concentrations, decreases $CO_2$, and increases pH; the opposite occurs in the afternoon (2, 3). Microbes can respond to changing conditions by acclimating or moving to more propitious environments by tracking chemical gradients (chemotaxis and aerotaxis) or light direction (phototaxis) (4, 5). Studying biofilm development in the lab has led to a distinction in bacterial life stages between a motile swarming phase vs a biofilm phase where cells are encased in a matrix and non-motile (6). However, other studies have demonstrated that surface-based motility can be important in determining biofilm structure (7, 8), that whole biofilm-like microcolonies can be motile (9), and that swarming and biofilm states can coexist, with motile cells entering and leaving aggregates (10). These observations suggest that bacteria may be quite motile within biofilms and microbial mats, which has consequences for how nutrients (11) and DNA (12) are transferred between species, and how the community responds to phage attack (13) or abiotic stress (14).

Several species of Cyanobacteriota (hereafter cyanobacteria) and Chloroflexota are abundant in hot spring microbial mats (15), core contributors to community metabolite fluxes (16), and thought to be the main determinants of mat architecture (17). Vertical distributions of cyanobacteria in mats vary over the diel cycle, suggesting migration in response to changing light, pH, or oxygen conditions (18, 19). Laboratory experiments have shown that filamentous and unicellular cyanobacteria can use Type IV pili (T4P) to move directionally in response to light gradients by phototaxis (20, 21). Chloroflexota isolates move by gliding motility (22) possibly driven by tight-adherence pili (23). How these species contribute or interact with each other to form biofilms is relatively unknown.

Current understanding of microbial mat structure is based mostly on examining in situ snapshots of species depth profiles (19, 24–26), while a few laboratory experiments have examined the motility of individual species (22, 27). We used the cyanobacterium *Synechococcus* sp. JA-2-3B′a(2-13) (28), originally isolated from Octopus spring in Yellowstone National Park (YNP) (recently proposed to be renamed *Thermostichus sp. JA-2-3Ba*) (29), and a member of the Chloroflexota, Chfl MS-1 (30), from the nearby Mushroom spring. Both species are abundant in several hot springs in YNP (31) and their motility, or that of close relatives, has been individually characterized to some extent (22, 27, 32). We reasoned that developing a binary consortium composed of these unicellular and filamentous species could allow us to examine the role of light and physical interactions in structuring “mat-like” biofilms.

We found that the binary consortium of Syn OS-B’ and Chfl MS-1 exhibited greater movement towards the light than either species individually. Replacing the wild-type Syn OS-B’ cells with a non-motile *ΔpilB* mutant, completely abrogated the cooperative effect suggesting that Syn OS-B’ motility was essential. Microscopy of the binary consortium revealed a physical association and parallel arrangement of Syn OS-B’ and Chfl MS-1 cells. Chfl MS-1 formed a more adherent

biofilm than Syn OS-B', and biofilm formation was increased further when the species were mixed. Inspection of binary consortia by electron microscopy revealed intercellular attachments, potentially facilitated by the secretion of extracellular polymeric substances (EPS). These binary consortia recapitulate some features of natural microbial mats and could be further developed t understand how mats are structured by dynamic light environments.

## Results

### Syn OS-B' and Chfl MS-1 are both motile on surfaces, but only Syn OS-B' is phototactic

Syn OS-B' grows as slightly curved rods 5-10 μm long and 2 μm wide (Figure S1A) , while Chfl MS-1 grows as an unbranched filament >100 μm long and 600 nm wide (Figure S1B). Transmission electron microscopy (TEM) of uranyl-acetate-stained whole cells revealed T4P located near the cell poles in Syn OS-B' (Figure S1C), and presumptive tight-adherence pili located near the septa between cells in a Chfl MS-1 filament (Figure S1D). Syn OS-B' and Chfl MS-1 contained chlorophyll A and bacteriochlorophyll c pigments, respectively (Figure S2), allowing them to be distinguished at a macroscopic scale.

To investigate Syn OS-B' and Chfl MS-1 motility, both species were grown separately to late log-phase in DH10M and PE medium, respectively, plated on DH10 solidified with 0.4% agarose at an adjusted $OD_{600}$=2, and incubated under either directional white light (60 μmol photons/$m^2$/s) (Figure S3) or in darkness for 4 days. Fluorescence scanning measurements showed Syn OS-B' (Figure 1A) and Chfl MS-1 (Figure 1G) have different collective motility patterns. Syn OS-B' moves towards the light while Chfl MS-1 moves in all directions with no apparent bias. Syn OS-B' increased its colony area only under directional light (Figure 1B), while Chfl MS-1 increased its colony area in both the light and dark (Figure 1H). Syn OS-B' cells were phototactic, forming parallel finger-like projections towards the light so that the center of the colony shifted towards the light by 2 mm (Figure 1C, Video S1), as described in greater detail in (32). Chfl MS-1 also produced collective projections composed of filament bundles, which formed more rapidly than those of Syn OS-B' but with no directional bias (Figure 1I, Video S2).

Individual Syn OS-B' cells exhibited "twitching motility" and primarily moved along their long axis (Figure 1D), which is typical of T4P-dependent surface motility in cyanobacteria (33). Chfl MS-1 filaments moved back and forth, parallel to their long axis, often forming bundles (Figure 1J). Syn OS-B' cells and Chfl MS-1 filaments exhibited similar speeds of 0.1-0.15 μm/s that did not differ between the light and dark (Figure 1E&K). Only Syn OS-B' cells developed a motility bias towards the light (Figure 1F&L). Syn OS-B' responded to illumination with a small and temporary (~20 second) increase in speed and a slower (~2 minute) development of motility bias, and to the dark transition with a temporary (~30 second) decrease in speed and gradual loss of motility bias (Video S3, Figure S4A&B). Chfl MS-1 speed and motility bias did not change under light transitions (Video S4, Figure S4C&D).

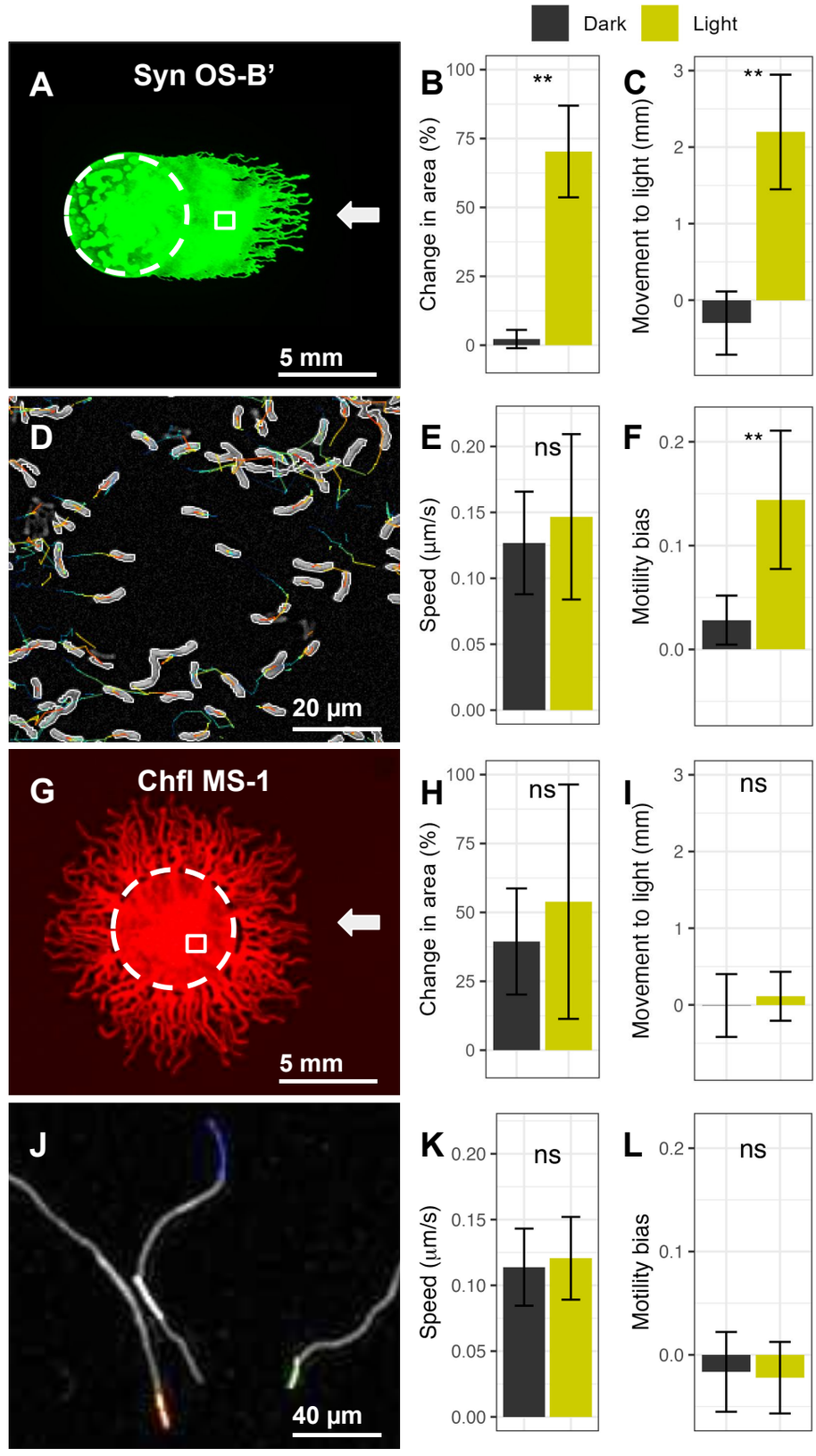


**Figure 1. Syn OS-B' and Chfl MS-1 are both motile, but only Syn OS-B' is phototactic. (A,G)** Fluorescence scan (ex. 658 nm / em. 710 nm) after 4 days of Syn OS-B' colony moving towards white light, and fluorescence scan (ex. 784 nm / em. 832 nm) of a colony of Chfl MS-1 after 4 days. White arrows indicate light direction, dashed circles indicate initial colony/droplet position, and the small box indicates an example region used for single-cell tracking in panels D and J. **(B,H)** Change in area of Syn OS-B' and Chfl MS-1 colonies on day 4 vs day 0. **(C,I)** Change in distance moved towards the light of Syn OS-B' and Chfl MS-1 colony centers on day 4 vs day 0. Data from 12 biological replicates in 2 experiments. **(D,J)** Microscope images of tracked Syn OS-B' cells and Chfl MS-1 filaments illuminated from the right, with coloured lines indicating tracks. In panel D, cells were tracked with Trackmate (Fiji) and paths coloured from blue to red over time, while in panel J, the tips of filaments were tracked with custom software (see methods) and each track given a unique color. **(E,K)** Speed of Syn OS-B' and Chfl MS-1 cells in the dark and light. **(F,L)** Motility bias (proportion of movement towards light) of Syn OS-B' and Chfl MS-1 cells. Data based on >100 Chfl MS-1 tips or >300 Syn OS-B' cells. Wilcoxon rank sum test was performed for each panel: ns=P>0.05, **=P<0.005.

**Interactions between Syn OS-B' and Chfl MS-1 enhance motility**

To explore physical interactions between species in the binary consortia, Syn OS-B' and Chfl MS-1 were mixed and exposed to directional white light on motility plates (Figure 2A). Chfl MS-1 projections emerged within 6 hours in all directions from the inoculation point, followed by Syn OS-B' moving towards the light after 12-24 hours (Video S5, Figure S5). This is similar to the behavior of each species when plated independently. However, in the binary consortium, Syn OS-B' moved mostly within the Chfl MS-1 projections towards the light and moved further than when alone (Figure 2B). Chfl MS-1 in the binary consortia also covered a larger area and moved further toward the light than Chfl MS-1 alone (Figure 2B and S5). To test the role of motility in this cooperative effect, and because the molecular details of cyanobacterial motility is quite well-understood (34), we focused on generating a non-motile mutant of Syn OS-B'. We identified CYB_2143 in Syn OS-B' as the homolog (58.3% amino acid identity) of the *Synechocystis* ATPase *PilB1* (slr0063), which is involved in pilus extension, and created knockout mutants using double homologous recombination (Figure S6A&B). These *ΔpilB* mutants still expressed genes up and downstream of *pilB* normally (Figure S7), lacked T4P when imaged by TEM (Figure S6C and S8&9), and exhibited no movement in standard photomotility assays (Figure S5D), confirming that *ΔpilB* was non-motile. When Chfl MS-1 was mixed in binary consortia with *ΔpilB*, Chfl MS-1 moved to the same extent as when alone, suggesting that the cooperative behavior in binary consortia required Syn OS-B' motility.

To determine whether some of this cooperative effect was caused by secreted substances, we collected spent media from cultures of Syn OS-B', *ΔpilB*, or Chfl MS-1 inoculated at OD600 nm = 1 and incubated for 24 hours. Spent media was passed through a 0.2 μm filter, and the filtrate added to the agarose surfaces prior to the motility assays. Only spent medium from Syn OS-B' had a statistically significant positive effect on the motility of Syn-OS-B' ($p<0.05$ after Bonferroni correction), although the median effect of *ΔpilB* or Chfl MS-1 spent media was also (not significantly) positive (Figure 2C). The motility of Chfl MS-1 was not significantly affected by spent media from any of the three cultures, consistent with the observation that *ΔpilB* cells, which can secrete but not move, did not improve Chfl MS-1 movement. This suggested that (i) Syn OS-B' motility may benefit more from secreted substances than Chfl MS-1, and (ii) direct physical interactions between motile Syn OS-B' and Chfl MS-1 (rather than their secretions) are likely the main contributors to the cooperative motility effect.

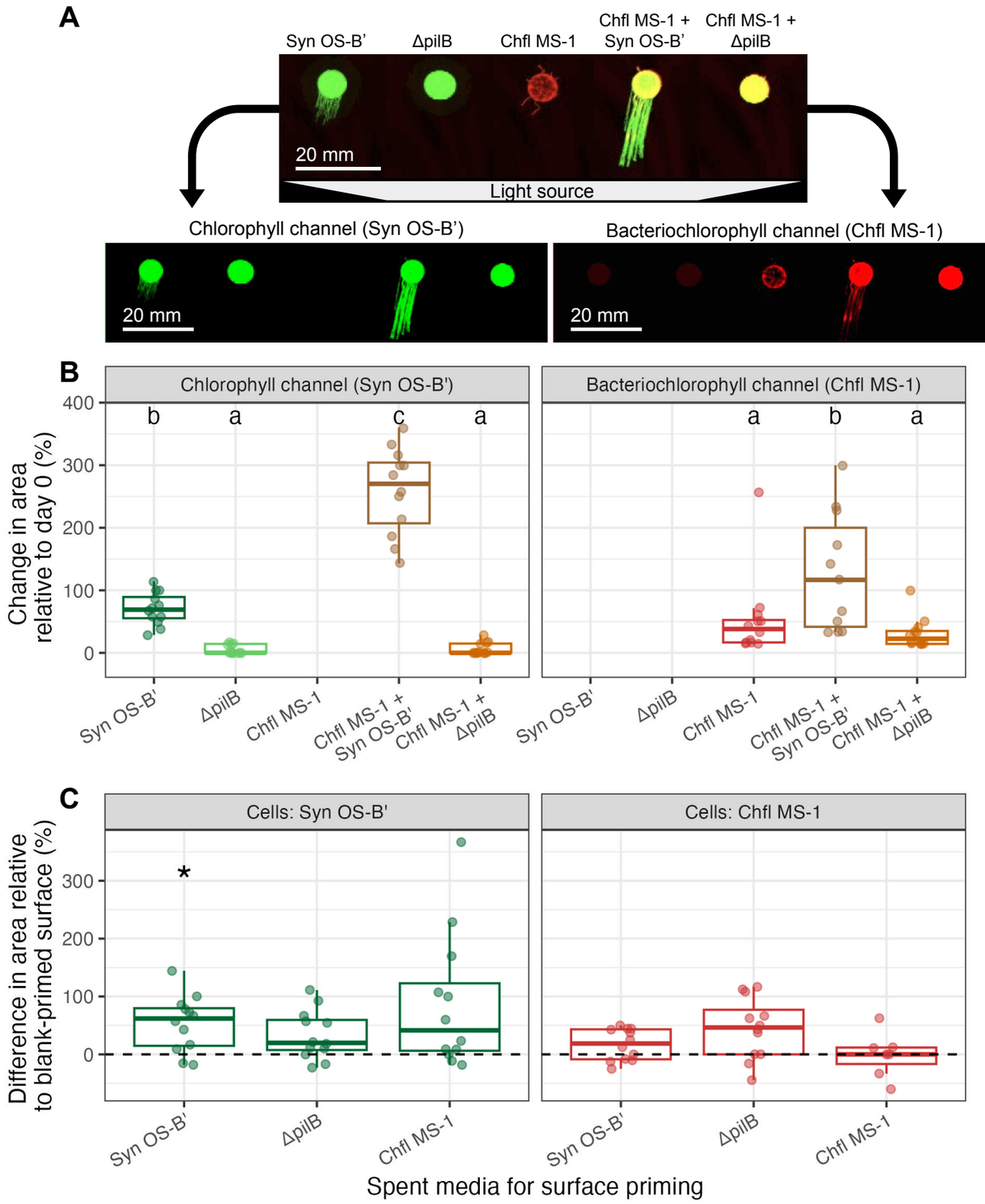


**Figure 2. Interactions between Syn OS-B' and Chfl MS-1 enhance motility. (A)** Fluorescent scans of Syn OS-B', *ΔpilB* mutant of Syn OS-B', Chfl MS-1, and binary consortia two days after exposure to directional white light. Top panel is the overlay of both fluorescence emission channels, and the bottom two panels represent Chlorophyll (ex. 658 nm / em. 710 nm) and Bacteriochlorophyll (ex. 784 nm / em. 832 nm) channels specific to Syn OS-B'/*ΔpilB* and Chfl MS-1, respectively. 5 raw images with standardized acquisition corresponding to each strain were combined prior to red-green channel separation. **(B)** Percent change in the covered colony area of Syn OS-B' or *ΔpilB* (left) and Chfl MS-1 (right) alone or in the binary consortia after 4 days of light relative to day 0. Compact letter display (letters at top of plot) indicates statistical differences at an adjusted *P* value of <0.05 in group means after Tukey's HSD test. (**C)** Percent difference in covered area of Syn OS-B' (left, green) or Chfl MS-1 (right, red) colonies on agarose surfaces primed with spent media from 24-hour cultures of Syn OS-B', *ΔpilB*, or Chfl MS-1, relative to surfaces primed with uninoculated fresh media (blank-primed surface). Data based on 7-12 biological replicates from 2 separate experiments. Student's T-tests with a null difference of 0 (dashed line) were performed with Bonferroni correction: *=P<0.05.

**Interactions between Syn OS-B' and Chfl MS-1 create ordered biofilms**

To investigate physical interactions between the species, we used fluorescence microscopy to visualize the cellular organization in Syn OS-B' colonies alone or with Chfl MS-1. Within Syn OS-B' projections towards the light, individual cells were often well separated and randomly oriented (Figure 3A&D). However, in the projections from binary consortia of Syn OS-B' and Chfl MS-1, the Syn OS-B' cells were organized in parallel arrays between Chfl MS-1 filaments (Figure 3B&E, Figure S10). When Syn OS-B' was replaced in the synthetic consortia by *ΔpilB*, *ΔpilB* cells were also packed in arrays but were less parallel to the light source and we noticed that a few *ΔpilB* cells were transported outside of the starting area (Figure 3C&F, Figure S11). The strong alignment of Syn OS-B' cells with the light direction in binary consortia suggests an interaction between motile Syn OS-B' and Chfl MS-1 cells.

Next, we investigated the consortia under light transitions. Under dark conditions, Chfl MS-1 filaments were prominent at the tip of the projection and moved around the Syn OS-B' cells (Video S6). However, after transitioning to the light, Syn OS-B' cells moved toward the light between Chfl MS-1 filaments, accumulated near the tip, and appeared to drive the projection toward the light. *ΔpilB* cells in binary consortia showed minimal movement in the dark or light (Video S7). Syn OS-B' cells at the tip of the projection were too densely packed to allow reliable cell tracking. However, in the middle of the positive phototactic projections, we could track Syn OS-B' using manually trained and automated image segmentation in ImageJ. As before, we preceded the cell tracking with a 10-minute dark incubation, after which Syn OS-B' cells in the phototactic projections were randomly oriented (mean angle of ~45° from the prior light source). Syn OS-B' cells with Chfl MS-1 were more parallel to the light (~15°) (Figure 3G). *ΔpilB* cells within binary consortia that had moved towards the light were selected for comparison, and showed only moderate light alignment of ~25° (Figure 3G). Upon directional illumination, axenic Syn OS-B' cells reoriented slightly toward the light (from 45° to 40°) and returned to a random orientation (45°) in the dark. Syn OS-B' and *ΔpilB* cells in binary consortia did not appear to reorient in the light, perhaps due to restrictions by Chfl MS-1 filaments (Figure 3G & Videos S8&9). Syn OS-B' cell speed was similar when alone or in binary consortia, but significantly higher than *ΔpilB* in consortia (Figure 3H). Some movement of *ΔpilB* cells was observed in binary consortia but this was likely due to the movement of neighboring Chfl MS-1 filaments. During the transition from light to dark conditions there was a noticeable but temporary decrease in Syn OS-B' speed, as previously observed (32), which was mitigated in binary consortia with Chfl MS-1, and not exhibited by *ΔpilB* (Figure 3H). As expected, Syn OS-B' increased its motility bias over the first 60-120 seconds of illumination when alone and in the binary consortium (Figure 3I), however, this bias declined after 120 seconds in both cases. The decline in Syn OS-B' bias was particularly striking in binary consortia suggesting that Chfl MS-1 may initially restrict Syn OS-B' movement. However, this is likely a temporary decline as the collective motility assays (Figure S5B) and longer videos (Video S6) indicated that Syn OS-B' continued to move steadily towards the light over longer periods.

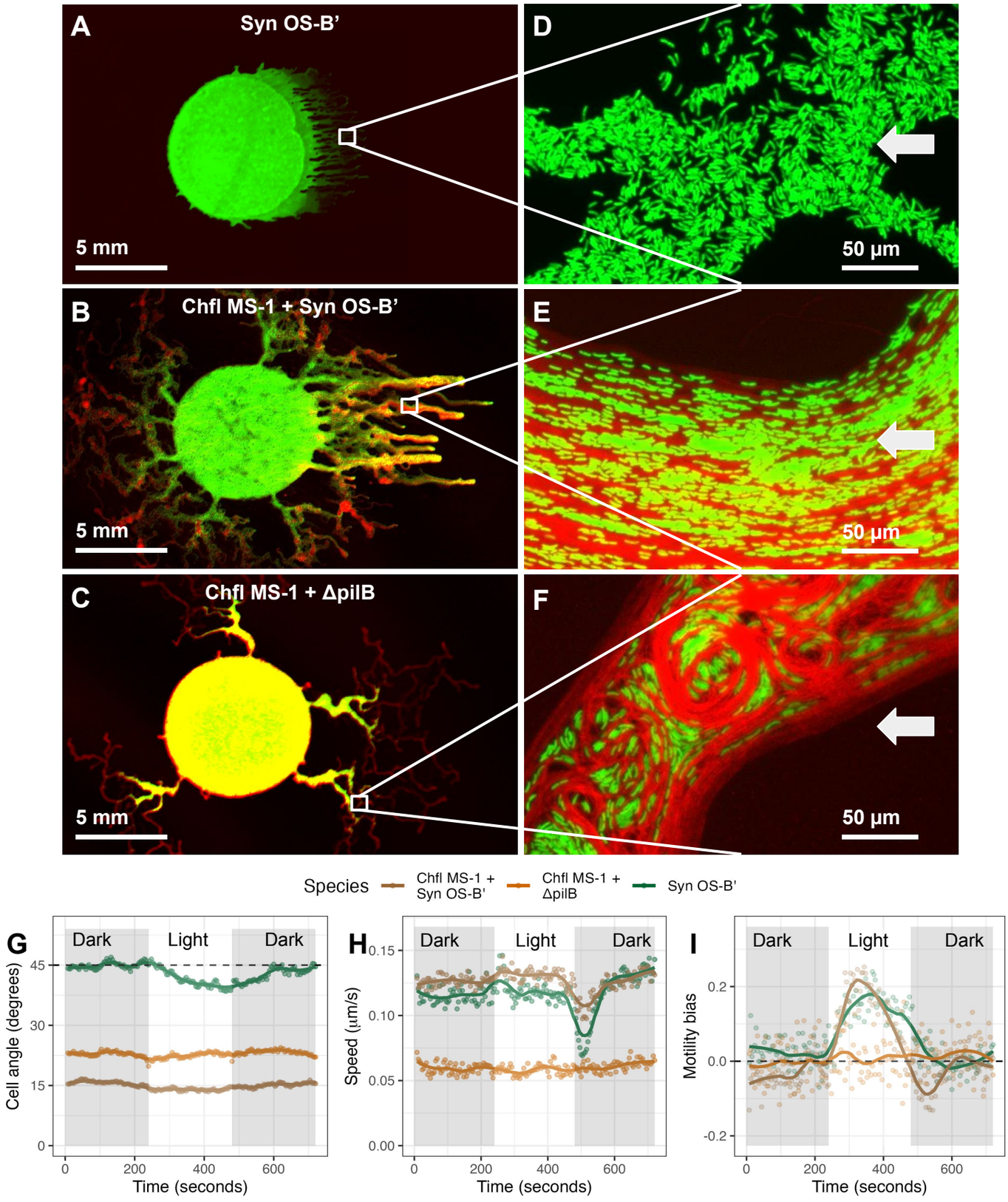


**Figure 3. Interactions between Syn OS-B' and Chfl MS-1 create ordered biofilms. (A-C)** Fluorescence scans of Syn OS-B' (top), Chfl MS-1 + Syn OS-B' (middle), and Chfl MS-1 + *ΔpilB* (bottom) after two days of incubation with white light from the right. Green regions = Syn OS-B' or *ΔpilB*, red regions = Chfl MS-1, yellow regions = both species. **(D-F)** Fluorescence microscope images of the indicated regions in panels A-C showing Syn OS-B' or *ΔpilB* rods in green (ex. 540-580 nm / em. 608-682 nm) and Chfl MS-1 filaments in red (ex.450-490 nm / em. >515 nm). **(G-J)** Dynamics of Syn OS-B' and *ΔpilB* movement during light transitions (gray regions=dark, white region=directional illumination with white light). Green = Syn OS-B', Brown = binary consortium of Chfl MS-1 + Syn OS-B', Orange = binary consortium of Chfl MS-1 + *ΔpilB*. **(G)** Average (mean) angle of the long axis of Syn OS-B' or *ΔpilB* cells relative to the light direction (0° = parallel, 45° = random, 90° = perpendicular) **(H)** Mean speed of Syn OS-B' or *ΔpilB* cells over time. **(I)** Motility bias of Syn OS-B' or *ΔpilB* cells over time. Data based on 10 biological replicates from 4 separate experiments with >300 total cells tracked at each time point per condition.

**Interactions between Syn OS-B' and Chfl MS-1 create stronger biofilms.**

We incubated Syn OS-B', *ΔpilB*, and Chfl MS-1 individually and in binary consortia in DH10 + 250 mg/L tryptone under constant white light in 384-well plate format, to observe biofilm formation on an inert surface. Imaging the bottom of the wells after 8 days (Figure 4A) showed various patterns. Syn OS-B' and *ΔpilB* produced a diffuse distribution pattern while Chfl MS-1 produced a reticulate network composed of bundles of filaments. In binary consortia, Syn OS-B' formed clusters within a Chfl MS-1 network, and *ΔpilB*-Chfl MS-1 binary consortia exhibited aggregation and colocalization of the two species. Next, we measured total culture density, density of the planktonic cells (resuspended by gentle pipetting), and biofilm-associated cells by crystal violet assay in 96-well tissue-culture treated plates. The total culture densities of the binary consortia and axenic Syn OS-B' and *ΔpilB* cultures were similar, but the Chfl MS-1 culture density was significantly lower (Figure 4B). The planktonic cell densities of the axenic Syn OS-B' and *ΔpilB* cultures were significantly higher than axenic Chfl MS-1 or the binary consortia, suggesting that Syn OS-B' and *ΔpilB* did not attach to the plate surface as well as Chfl MS-1, and that the presence of Chfl MS-1 improved their retention in the biofilm (Figure 4B). Indeed, in the consortia, the biofilm levels were significantly higher than any of the single-species cultures (Figure 4B). We also measured the dynamics of biofilm formation over four days. We found detectable biofilm levels after 6 hours (Figure S12), with maximal biofilm development occurring between 6-24 hours, concurrent with a decrease in the planktonic fraction.

To visualize physical interactions within the biofilm, we prepared binary consortia of Syn OS-B' and Chfl MS-1 in liquid culture for scanning (SEM), transmission electron microscopy (TEM), and cryo-electron microscopy (cryo-EM). SEM images revealed a close association between Syn OS-B' and Chfl MS-1, with Chfl MS-1 filaments forming the bulk of the biofilm (Figure 4C & S13). TEM images of the associations at higher resolution showed increased electron density between the cells. This might be interpreted as secreted EPS between species but needs further experimentation (Figure 4D & S14) (35). Cryo-EM revealed a fuzzy external layer on the surface of Chfl MS-1 cells and many pilus-like structures between Syn OS-B' and Chfl MS-1 (Figure 4E). Together, these results suggest that Chfl MS-1 and Syn OS-B' establish tight interactions producing a more robust biofilm when together.

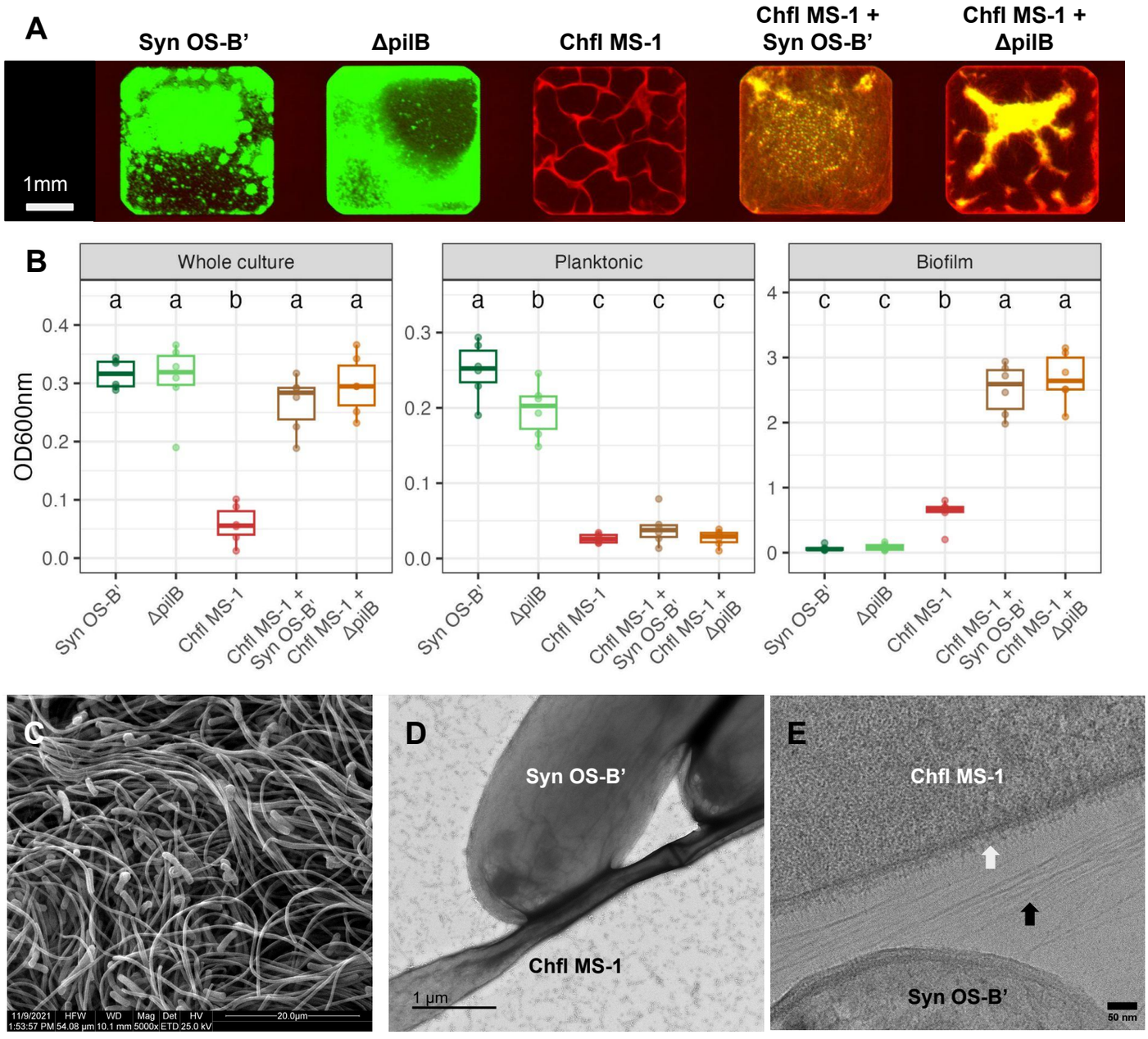


**Figure 4. Interactions between Syn OS-B' and Chfl MS-1 create stronger biofilms. (A)** Representative scanning fluorescence images of the bottom of culture wells in a multiwell plate after 8 days growth in DH10 + 250 mg/L tryptone. Green regions indicate Syn OS-B' (ex. 658 nm / em. 710 nm), red regions indicate Chfl MS-1 (ex. 784 nm / em. 832 nm). **(B)** Boxplot and individual measurements of OD600nm values from various fractions of the cultures: whole culture (left), planktonic fraction (middle), biofilm fraction after crystal violet assay (right). Data based on 6 biological replicates from one experiment with additional data in Figure S12. Compact letter display (letters at top of plot) indicates statistical differences at $P<0.05$ in group means after Tukey's HSD test. **(C)** Syn OS-B'-Chfl MS-1 samples imaged by SEM at 5000x. **(D)** Syn OS-B'-Chfl MS-1 samples stained with uranyl-acetate and imaged by TEM at 30,000x. **(E)** Syn OS-B'-Chfl MS-1 samples plunge-frozen in liquid ethane, milled by cryogenic focused-ion bean SEM (cryoFIB-SEM), and then imaged by cryo-EM. White arrow indicates a fuzzy external layer (EL) [23] to the cell membrane of Chfl MS-1. Black arrow indicates long, thin, pili-like filaments (6-8 nm diameter).

262 **Discussion**
263
264 We investigated how bacterial motility responses to light can shape the architecture of microbial
265 mats using two dominant members of Yellowstone hot spring mat communities. We found
266 comparable behavior of Syn OS-B' and Chfl MS-1 to other observed Cyanobacteria and
267 Chloroflexota. By studying the motility and arrangement of these species in binary consortia, we
268 revealed some unique emergent properties. These insights could enhance our understanding of
269 the dynamics of natural microbial mat architecture, and help to develop synthetic consortia for
270 uses in industry.
271
272 **Syn OS-B' and Chfl MS-1 behavior is comparable to other Cyanobacteria and**
273 **Chloroflexota**
274 Chfl MS-1 exhibited surface motility at speeds consistent with other hot spring Chloroflexota
275 (36), and formed gliding aggregates of filaments similar to *Chloroflexus aggregans (37)*. Chfl
276 MS-1 did not exhibit phototaxis, which, to our knowledge, has not been reported in the
277 Chloroflexota, however, light does increase *C. aggregans* aggregation rate (38). The genes
278 responsible for Chfl MS-1 motility were not investigated here, but the Chfl MS-1 genome (30)
279 does contain TadE/G genes of the tight adherence pilus family, which is involved in the motility
280 of *Liberibacter crescens (39)*.
281
282 As we reported previously (32), Syn OS-B' was similar in speed and phototactic bias to other
283 characterized cyanobacteria, particularly those from Yellowstone hot springs (27). Here, we
284 found that disruption of the homolog of *pilB* in Syn OS-B' (CYB_2143), resulted in loss of T4P
285 and motility, as found in *Synechocystis* sp. PCC 6803 (40). Syn OS-B' did not form adherent
286 biofilms, as observed in laboratory strains of model cyanobacteria such as *Synechocystis* PCC
287 6803 and *Synechococcus elongatus* PCC 7942 grown under normal conditions, but differing
288 from some related wild isolates, which do form biofilms (41, 42). The mutant lacking *pilB* was
289 slightly less abundant in the planktonic phase than Syn OS-B', suggesting that pili might prevent
290 cell sinking, as observed in marine cyanobacteria (43), or inhibit biofilm formation, as found in *S.*
291 *elongatus* (44).
292
293 **A unique synthetic system for studying emergent biofilm properties**
294 This binary consortium has relatively unique features useful for mixed-species biofilm research,
295 including: (i) strains recently isolated from well-studied microbial mats, with few generations to
296 acquire laboratory mutations; (ii) a member (Syn OS-B') that is naturally transformable allowing
297 mutant generation to test gene function e.g. *ΔpilB*; (iii) two members with different morphologies
298 (rod-shaped vs filamentous), motilities (phototactic twitching vs gliding), and fluorescent
299 pigments (allowing species to be distinguished); and (iv) emergent or cooperative properties in
300 both surface motility and biofilm formation when the species are combined.
301
302 Cooperative microbial motility often depends on the release of surfactants, such as rhamnolipids
303 in *P. aeruginosa (45)*. We found that Syn OS-B' motility was slightly improved by supplementing
304 the agar surface with Syn OS-B' spent medium suggesting Syn OS-B' surfactant production
305 may limit its surface motility. Indeed, the finger-like collective projections we observed for Syn

306 OS-B' can indicate collective movement limited by surfactant production (46). Nonetheless,
307 direct physical interactions between cells appear crucial to the cooperative effect. This might
308 partly be explained by the branching-exploratory behavior of Chfl MS-1, which can maximize
309 colonization (47), combined with the phototactic directionality of Syn OS-B'. Importantly, Chfl
310 MS-1 exhibited the emergent property of positive bias towards the light only when mixed with
311 Syn OS-B'. Mathematical models that incorporate morphological information, directional bias,
312 and the effect of motility-promoting substances could be useful for understanding this
313 cooperative phenomenon.
314
315 Mixed-species biofilms are often more disordered than single-species biofilms and less robust,
316 for example to predation or invasion (48, 49). By contrast, we found that Syn OS-B' was more
317 ordered and aligned with the light source when mixed with Chfl MS-1 than when alone. This
318 may result from repeated collisions between Chfl MS-1 filaments and the phototactic Syn OS-B'
319 rods leading to the alignment in the primary direction of movement. This long-range ordering via
320 collisions has been observed in biofilms of filamentous *E. coli* (50), and in mathematical models
321 based on filamentous cyanobacteria (51). Statistical models of biofilm architecture have found
322 that the cellular length:width ratio is amongst the most important determinants of biofilm
323 structure (52), corroborating the finding that filamentous Chfl MS-1 had a large impact on Syn
324 OS-B' arrangement.
325
326 In addition to increased motility, we observed higher biofilm formation in the binary consortia
327 than axenic cultures. Increased biofilm formation in species mixtures has been found in bacteria
328 isolated from the soil and human gut (53, 54). In our case, this is at least partly due to stronger
329 aggregation and substrate attachment in binary consortia, rather than just increased growth, as
330 Syn OS-B' and *ΔpilB* decline in the planktonic fraction when mixed with Chfl MS-1. Chfl MS-1
331 formed biofilms when alone, suggesting it is the driver of biofilm adherence. This agrees with
332 other findings that filamentous cells often form the biofilm core or help stabilize its structure (55).
333
334 **Cyanobacteria-Chloroflexota biofilms in natural and industrial settings**
335 In hot springs, Chloroflexota are reported to mainly acquire organic carbon from cyanobacteria,
336 often as excreted organic acids (56, 57). Moving and associating with cyanobacteria may
337 therefore provide an advantage for Chloroflexota. Indeed, vertically oriented Chloroflexota
338 filaments have been observed amongst cyanobacterial cells in hot spring mats, particularly
339 during mat regrowth (17), potentially suggesting alignment by phototactic cyanobacteria moving
340 towards or away from the light. Alternatively, vertical migrations of Chloroflexota in Octopus
341 spring mats might also be due to positive aerotaxis (17), which has been characterized in
342 *Chloroflexus aggregans* in the laboratory (58). We performed motility experiments on soft
343 agarose surfaces exposed to air in part to avoid the potential confounding effect of oxygen
344 gradients. However, future studies could recapitulate three-dimensional biofilm architecture in
345 microfluidic devices with flow, and extend our photomotility experiments to more complex and
346 realistic environments.
347
348 Chloroflexota are considered the main contributors to mat structure in several Yellowstone hot
349 springs because they are abundant in structures above the mat surface such as 'nodules' or

350 ‘streamers’, and continue to form a mat when cyanobacteria are diminished (17). This is
351 consistent with our results that Chfl MS-1 can form strong biofilms without Syn OS-B’ but not
352 vice versa. However, Boomer *et al.* found that *Synechococcus* and *Thermus* were the first
353 genera to form biofilms on glass rods suspended above hot spring mats, with Chloroflexota and
354 filamentous cyanobacteria only contributing to the biofilm months later (59). Future work could
355 therefore test the motility and biofilm formation of other mat members, either in isolation or in
356 mixed-species biofilms. It is also important to note that many microbial mats are dominated by
357 filamentous cyanobacteria (18, 60), which may form adherent biofilms and long-range order
358 without interacting with other filamentous species.
359
360 Chloroflexota and Cyanobacteria don’t only associate in natural habitats. Zhang *et al.* found
361 they were the main contributors to nutrient removal in municipal wastewater treatment
362 photobioreactor experiments (61). These phyla have each received considerable attention in
363 wastewater treatment (62, 63), and it has been suggested that their combination could provide
364 advantages of reduced greenhouse gas emissions and better surface adherence or settleability
365 to reduce biomass separation costs (64, 65). Cyanobacterial biofilm formation also offers
366 advantages in increasing bioenergy and biofuel productivity (66), and the addition of
367 heterotrophic strains can increase cyanobacterial attachment (67). Our results that binary
368 consortia of cyanobacteria and Chloroflexota isolates cooperate to form robust biofilms may
369 therefore inform phototrophic biofilm cultivation strategies for commercial applications.
370
371 **Conclusion**
372
373 We found that Cyanobacteria and Chloroflexota isolates that co-occur in hot springs show
374 different motility responses to light but can cooperate to form robust biofilms and migrate over
375 larger distances. These results provide insights into physical interactions within hot spring mats
376 and highlight understudied features of biofilm communities, including directional movement via
377 phototaxis, the emergence of long-range cellular order, and cooperation in both motility and
378 biofilm formation.
379
380 **Methods**
381
382 **Strains and culture conditions**
383
384 *Synechococcus* sp. JA-2-3B′a(2-13) (OS-B′) was originally isolated by filter cultivation from a
385 51-61°C Octopus Spring mat core sample (Bhaya et al. 2007). *Chloroflexus* sp. MS-CIW-1 was
386 isolated from a 60°C Mushroom Spring mat core sample by serially picking colonies and
387 streaking them on PE medium (0.4% agarose) plates. Both strains were stored at −70°C in 20%
388 (wt/vol) glycerol stocks prior to culturing. Syn OS-B’ cultures were maintained in DH10M
389 medium (medium D (68) plus 10 mM HEPES adjusted to pH 8.2, with added 250 $mg \cdot L^{-1}$ bacto-
390 tryptone, and 750 $mg \cdot L^{-1}$ sodium bicarbonate). Chfl MS-1 was maintained in PE medium (69).

Both species were incubated at 50°C under continuous light at 50 μmol·m$^{-2}$·s$^{-1}$ (measured with a LI-COR [model Li-189] radiometer) in an Algaetron ag130 incubator (Photon Systems Instruments) or similar incubators. To determine axenicity, we plated the cultures, incubated them on DH10M agarose plates with added yeast extract (100 mg·L$^{-1}$) and checked for any non-Syn OS-B' or non-Chfl MS-1 colonies.

**Collective motility assay**

Cultures in late-log phase (OD600nm of Syn OS-B' and Chfl MS-1 of ~0.6 and ~0.3, respectively) were concentrated to an OD600nm of 2.0 using a spectrophotometer (Tecan M1000 Pro), centrifugation, and resuspension in DH10 (medium D (68) plus 10 mM HEPES adjusted to pH 8.2). 5 μL of these concentrated cultures were plated on DH10 solidified with 0.4% (wt/vol) agarose in bacteriological petri dishes with tightly fitting lids (Falcon 25369-022) and allowed to dry for ~10 min in a laminar flow cabinet. Plates were then inverted and incubated at 50°C with unidirectional daylight white LED illumination (spectrum in Figure S3) at 60 μmol·m$^{-2}$·s$^{-1}$. Plates were imaged using a fluorescent scanner (Azure biosystems) at 0, 6, 24, 48, 72, and 96 hours after incubation. Two fluorescent channels were used: excitation at 658 nm or 784 nm with emission capture at 710 nm or 832 nm with 40 nm bandpass for Syn OS-B' or Chfl MS-1, respectively. Images were processed using custom ImageJ macros to identify the regions where Syn OS-B' and Chfl MS-1 had moved. The experimental setup metadata file describing where drops were placed on the plates and this extracted colony distribution data were matched using the Hungarian algorithm for solving the linear sum assignment problem in R version 4.3.1.

**Single-cell time lapse video microscopy**

Single-cell motility measurements were captured by Time-lapse video microscopy (TLVM). The temperature was maintained at 50°C using a custom environmental chamber (HaisonTech), and illumination provided by rows of white LEDs (spectra in Figure S1) positioned 10 cm from and at 5° above the agarose surface. The light intensity measured at the cells' position was 60 μmol·m$^{-2}$·s$^{-1}$. Cells were prepared as described above for collective phototaxis measurements with Chfl MS-1 filaments tracked from a lower density droplet within hours after plating, while Syn OS-B' cells were tracked after 2-4 days and amongst cells that had already displayed positive phototaxis. All petri dishes remained closed and inverted during recording with a minimum 10-minute incubation at 50°C in darkness prior to the 4- to 12-minute recordings at ×200 magnification and 10-15 frames per minute. All videos were made using a Nikon Eclipse TE300 inverted microscope attached to a Coolsnap Pro monochrome camera (Media Cybernetics, Silver Spring, MD, USA), and images were collected by MetaMorph software (v4.6r5 and 6.2r6; Molecular Devices). Example videos can be found at https://www.youtube.com/channel/UCX0gm-79tZplREzHteapEWA.

**Syn OS-B' tracking**

434 Image stacks were preprocessed using Image J v1.53f51 (70) by subtracting the background
435 with a rolling ball radius of 4. Cells were tracked using the ImageJ plugin Trackmate (71) with a
436 thresholding filter applied and filtering to blobs of >25 pixels. The Kalman tracker was selected
437 with the initial search radius set to 15, the subsequent search radii to 15, and the maximum
438 frame gap to 3. The "spots" file was exported to csv and imported into R version 4.3.1 for
439 preprocessing and analysis (72). Speed was calculated as distance (in μm)/time (in s). Motility
440 bias was calculated as parallel displacement (in μm)/distance (in μm).
441
442 **Chfl MS-1 tracking**
443
444 We developed a custom tracking algorithm for filamentous bacterial tracking in LabView
445 programming language, with a convenient user interface. The timelapse 2D images were
446 corrected by pixelization, integrated FFT noise filtering, simple Kalman filtering, adjacent pixel
447 averaging and 4th-degree polynomial curve correction in X direction and adaptive pixel intensity
448 inversion to ensure that bacterial intensity is above the background. The tracking was performed
449 on the original frame on 10 filaments per video. The filament ends were picked manually by
450 positioning the cursor in an interactive image and after thresholding, the algorithm tracked the
451 filament tip between frames. The end pixels were found by the "grassfire" method and their
452 center of mass was taken as the true end. The tracks were plotted in real time with a set delay,
453 to view the tracking quality in real time and ensure fidelity. After the last frame, the tracks were
454 saved in a text file and analyzed in R version 4.3.1 to calculate speed and motility bias as
455 above.
456
457 **Biofilm quantification**
458
459 Biofilm formation was quantified using the crystal violet assay (73), with modifications as in (74).
460 Briefly, Syn OS-B', *ΔpilB*, Chfl MS-1, and binary consortia were inoculated at OD600nm of 0.4
461 into DH10 or DH10 + BT media in 96-well polystyrene plates and incubated under continuous
462 white light at 50 $\mu mol \cdot m^{-2} \cdot s^{-1}$ and 50°C. After 0-4 days of incubation, OD600nm absorption
463 measurements were taken on the total culture. Then, cultures were briefly disrupted by
464 pipetting, and 80% of the culture volume was transferred to a new plate. OD600nm was
465 measured in the 20% of the remaining volume and called "Non-planktonic OD600nm", and in
466 the transferred volume, called "Planktonic OD600nm". Plates were washed three times by
467 adding 200 μl of Milli-Q water, pipetting up and down, then removing and discarding 200 μl.
468 Then, 200 μl of aqueous 0.1% crystal violet was added to each well and the plate incubated at
469 room temperature for 20 minutes. Plates were washed 3 times with Milli-Q water as before, then
470 200 μl of 95% ethanol was added to each well and the plate agitated for 5 minutes. OD600nm
471 was then recorded and reported as the Biofilm (CV) level.
472
473 **Scanning electron microscopy**
474
475 A 5 μl aliquot of a late log phase culture of Syn OS-B' + Chfl MS-1 was added to the surface of
476 an SEM stub (Ted Pella), and a Kimwipe tissue (Kimtech) was used to blot away excess liquid.
477 The SEM stub was then immersed in 100% methanol for 5 minutes, rinsed with 100% ethanol,

and immersed in ethanol for 10 minutes. The SEM stubs then underwent critical point drying with $LCO_2$ in DCP-1 (Denton Vacuum) in 200-proof ethanol at a maximum of 50-60℃ and 9-10 MPa, with depressurization at 300-700 kPa per minute. Gold sputtering from pure Au target was performed in Denton Desk IV (Denton Vacuum) under argon gas at a pressure of 6 kPa for 200 seconds and a low current of 7 mA. The samples were imaged in Quanta 200 (FEI) SEM with 25 kV accelerating voltage in high vacuum with secondary emission detector.

**Transmission electron microscopy**

300 mesh Formvar and carbon-coated copper grids (FCF300-Cu, Ted Pella) were irradiated with low-energy Al plasma glow to create a hydrophilic surface in Denton Desk II instrument (Denton Vacuum). The Syn OS-B' + Chfl MS-1 binary consortium was gently mixed and 5 µl drops were deposited on the shiny side of the grids and left for 3 minutes before negative staining was performed using standard methods. This involved dipping the grid face-down consecutively onto two DI $H_2O$ droplets, followed by rinsing in 3 drops of 1% uranyl acetate, and resting to stain for 1 minute before blotting away the remaining uranyl acetate and leaving the sample to dry completely. The grids with bacteria were imaged in JEOL JEM-1400 with 120 kV accelerating voltage equipped with a Gatan Inc. OneView 4kX4k sCMOS camera.

**Cryo-electron microscopy**

A binary consortium of Chfl MS-1 and Syn OS-B' was grown for 6 days in DH10 medium in a sealed 96 well plate at 50°C and under 12:12hr light-dark cycles with LED daylight white illumination at 60 $\mu mol \cdot m^{-2} \cdot s^{-1}$. After 11 hrs of the dark period, the biofilm was resuspended gently by pipetting, diluted 9-fold in DH10, and 3 µl of cell suspension transferred onto 200 mesh Carbon Quantifoil R1.2 Gold TEM grids, which were glow-discharged using a Pelco EasiGlow to enhance hydrophilicity. Cells were allowed to settle for 30 seconds, followed by single-sided blotting for 4-8 seconds and vitrification in liquid ethane using a Leica EM GP2 robotic plunge-freezer. Samples were transferred cryogenically into a Thermo Fisher Aquilos2 Dual Beam cryogenic focused ion beam scanning electron microscope (cryo-FIB/SEM) to generate 200 nm thin lamellae. The stage temperature was -185 °C to maintain vitreous ice during milling. Grids were sputter-coated with platinum for 25 seconds, followed by a protective layer of organo-platinum for 2 minutes using the integrated gas injection system. Milling was performed with the Gallium-ion beam at 30 kV and currents decreasing from 500 to 13 pA until 500 nm thickness, then at 10 pA to 200-300 nm. SEM inspection of the lamellae and final polishing was conducted with a 2 kV and 13-25 pA electron beam. Samples were transferred to a Thermo Fisher Titan Krios G3i cryo-TEM and screening images were collected using SerialEM 4.11.12 on a K3 direct electron detector (Gatan Inc.) with a Bioquantum energy filter using 20 eV slit width. Images were collected at 42,000x nominal magnification with 2.6 Å/pix, an exposure of 0.3 seconds, and a defocus of -3 µm. Images were binned 4x for visualization, and ultrastructure measurements were performed using IMOD 4.11.12 (75) or FIJI (70).

**Acknowledgments**

F.B. acknowledges support from the University of Chicago, Carnegie Institution for Science, and a BBSRC-NSF/BIO collaborative research grant (award number 1921429). V.C. was supported by a grant from the National Aeronautics and Space Administration (80NSSC19K0462). C.R., D.B., and A.G. acknowledge support from NSF/BIO 1921429 and from the Carnegie Institution for Science. This research was partially supported by the DOE Office of Biological and Environmental Research, Biological Systems Science Division, FWP 74915, and by NIH S10 Award Number 1S10OD028536-01 from the Office of Research Infrastructure Programs (ORIP). Part of this research was performed on a project award (10.46936/expl.proj.2021.60171/60008194) from the Environmental Molecular Sciences Laboratory, a DOE Office of Science User Facility sponsored by the Biological and Environmental Research program under Contract No. DE-AC05-76RL01830. Some of this work was performed at the Stanford-SLAC Specimen Preparation Center (SCSC), which is supported by the National Institutes of Health Common Fund's Transformative High-Resolution Cryoelectron Microscopy Program (U24GM139166). We thank the Yellowstone National Park Service and David Ward for sampling permit #YELL-5494 awarded to David Ward and Devaki Bhaya, which allowed the collection of mat samples from which Chfl MS-1 and Syn OS-B' were isolated. We also thank Stanford CSIF and Carnegie Advanced Imaging Facility for access to their TEM and SEM instruments.

**Author contributions**

F.B., A.G,.and D.B. designed the research. F.B., C.R., V.C., and A.M. performed experiments. A.M., L.M.J, A.D.P, and J.E.M. provided tools, sample processing, and performed microscopy analysis on samples. F.B. and D.B. analyzed the results and wrote the manuscript with input from all authors.

**Competing Interests**

The authors declare no competing financial interests.

**Data availability statement**

All data presented in this manuscript are available in the supplementary data files along with an R script to reproduce all plots and statistical tests.

**References**

1. W.-S. Shu, L.-N. Huang, Microbial diversity in extreme environments. *Nat. Rev. Microbiol.* 1–17 (2021).

2. L. J. Stal, Physiological ecology of cyanobacteria in microbial mats and other communities. *New Phytol.* **131**, 1–32 (1995).

3. S. I. Jensen, A.-S. Steunou, D. Bhaya, M. Kühl, A. R. Grossman, In situ dynamics of O2, pH and cyanobacterial transcripts associated with CCM, photosynthesis and detoxification

565 of ROS. *ISME J.* **5**, 317–328 (2011).

566 4. J. M. Keegstra, F. Carrara, R. Stocker, The ecological roles of bacterial chemotaxis. *Nat.*
567 *Rev. Microbiol.* **20**, 491–504 (2022).

568 5. A. Wilde, C. W. Mullineaux, Light-controlled motility in prokaryotes and the problem of
569 directional light perception. *FEMS Microbiol. Rev.* **41**, 900–922 (2017).

570 6. K. Sauer, *et al.*, The biofilm life cycle: expanding the conceptual model of biofilm formation.
571 *Nat. Rev. Microbiol.* **20**, 608–620 (2022).

572 7. P. Chiang, L. L. Burrows, Biofilm formation by hyperpiliated mutants of Pseudomonas
573 aeruginosa. *J. Bacteriol.* **185**, 2374–2378 (2003).

574 8. M. Klausen, A. Aaes-Jørgensen, S. Molin, T. Tolker-Nielsen, Involvement of bacterial
575 migration in the development of complex multicellular structures in Pseudomonas
576 aeruginosa biofilms. *Mol. Microbiol.* **50**, 61–68 (2003).

577 9. C. Li, *et al.*, Social motility of biofilm-like microcolonies in a gliding bacterium. *Nat.*
578 *Commun.* **12**, 5700 (2021).

579 10. V. M. Worlitzer, *et al.*, Biophysical aspects underlying the swarm to biofilm transition. *Sci*
580 *Adv* **8**, eabn8152 (2022).

581 11. K. A. Brileya, L. B. Camilleri, G. M. Zane, J. D. Wall, M. W. Fields, Biofilm growth mode
582 promotes maximum carrying capacity and community stability during product inhibition
583 syntrophy. *Front. Microbiol.* **5**, 693 (2014).

584 12. L. Ma, M. E. Konkel, X. Lu, Antimicrobial Resistance Gene Transfer from Campylobacter
585 jejuni in Mono- and Dual-Species Biofilms. *Appl. Environ. Microbiol.* **87**, e0065921 (2021).

586 13. N. K. Ratheesh, A. M. Zdimal, C. A. Calderon, A. Shrivastava, Bacterial Swarm-Mediated
587 Phage Transportation Disrupts a Biofilm Inherently Protected from Phage Penetration.
588 *Microbiol Spectr* **11**, e0093723 (2023).

589 14. R. G. Perkins, *et al.*, Vertical cell movement is a primary response of intertidal benthic
590 biofilms to increasing light dose. *Mar. Ecol. Prog. Ser.* **416**, 93–103 (2010).

591 15. J. M. Wood, *et al.*, Assessing microbial diversity in Yellowstone National Park hot springs
592 using a field deployable automated nucleic acid extraction system. *Frontiers in Ecology and*
593 *Evolution* **12** (2024).

594 16. L. Steinke, *et al.*, Short-Term Stable Isotope Probing of Proteins Reveals Taxa
595 Incorporating Inorganic Carbon in a Hot Spring Microbial Mat. *Appl. Environ. Microbiol.* **86**
596 (2020).

597 17. W. N. Doemel, T. D. Brock, Structure, growth, and decomposition of laminated algal-
598 bacterial mats in alkaline hot springs. *Appl. Environ. Microbiol.* **34**, 433–452 (1977).

599 18. M. Lichtenberg, P. Cartaxana, M. Kühl, Vertical migration optimizes photosynthetic
600 efficiency of motile cyanobacteria in a coastal microbial mat. *Frontiers in Marine Science*
601 (2020).

19. N. B. Ramsing, M. J. Ferris, D. M. Ward, Highly ordered vertical structure of Synechococcus populations within the one-millimeter-thick photic zone of a hot spring cyanobacterial mat. *Appl. Environ. Microbiol.* **66**, 1038–1049 (2000).

20. S. Yoshihara, M. Ikeuchi, Phototactic motility in the unicellular cyanobacterium Synechocystis sp. PCC 6803. *Photochem. Photobiol. Sci.* **3**, 512–518 (2004).

21. P. Italia, V. K. Pallipuram, D. D. Risser, Dynamic localization of HmpF regulates type IV pilus activity and directional motility in the filamentous cyanobacterium Nostoc punctiforme. *Molecular* (2017).

22. S.-I. Fukushima, S. Morohoshi, S. Hanada, K. Matsuura, S. Haruta, Gliding motility driven by individual cell-surface movements in a multicellular filamentous bacterium Chloroflexus aggregans. *FEMS Microbiol. Lett.* **363** (2016).

23. V. A. Gaisin, R. Kooger, D. S. Grouzdev, V. M. Gorlenko, M. Pilhofer, Cryo-Electron Tomography Reveals the Complex Ultrastructural Organization of Multicellular Filamentous Chloroflexota (Chloroflexi) Bacteria. *Front. Microbiol.* **11**, 1373 (2020).

24. A. Fourçans, *et al.*, Vertical migration of phototrophic bacterial populations in a hypersaline microbial mat from Salins-de-Giraud (Camargue, France). *FEMS Microbiol. Ecol.* **57**, 367–377 (2006).

25. E. D. Becraft, F. M. Cohan, M. Kühl, S. I. Jensen, D. M. Ward, Fine-scale distribution patterns of Synechococcus ecological diversity in microbial mats of Mushroom Spring, Yellowstone National Park. *Appl. Environ. Microbiol.* **77**, 7689–7697 (2011).

26. L. Wörmer, *et al.*, A micrometer-scale snapshot on phototroph spatial distributions: mass spectrometry imaging of microbial mats in Octopus Spring, Yellowstone National Park. *Geobiology* **18**, 742–759 (2020).

27. N. B. Ramsing, M. J. Ferris, D. M. Ward, Light-induced motility of thermophilic Synechococcus isolates from Octopus Spring, Yellowstone National Park. *Appl. Environ. Microbiol.* **63**, 2347–2354 (1997).

28. J. P. Allewalt, M. M. Bateson, N. P. Revsbech, K. Slack, D. M. Ward, Effect of temperature and light on growth of and photosynthesis by Synechococcus isolates typical of those predominating in the octopus spring microbial mat community of Yellowstone National Park. *Appl. Environ. Microbiol.* **72**, 544–550 (2006).

29. J. Komárek, J. R. Johansen, J. Šmarda, O. Strunecký, Phylogeny and taxonomy of Synechococcus-like cyanobacteria. *Fottea* **20**, 171–191 (2020).

30. A. N. Shelton, *et al.*, Draft genome of Chloroflexus sp. MS-CIW-1, of the Chloroflexus sp. MS-G group from Mushroom Spring, Yellowstone National Park. *Microbiol Resour Announc* **13**, e0071023 (2024).

31. A. C. Bennett, S. K. Murugapiran, T. L. Hamilton, Temperature impacts community structure and function of phototrophic Chloroflexi and Cyanobacteria in two alkaline hot springs in Yellowstone National Park. *Environ. Microbiol. Rep.* **12**, 503–513 (2020).

32. F. Bunbury, *et al.*, Differential Phototactic Behavior of Closely Related Cyanobacterial

641 Isolates from Yellowstone Hot Spring Biofilms. *Appl. Environ. Microbiol.* **88**, e0019622
642 (2022).

643 33. M. Burriesci, D. Bhaya, Tracking phototactic responses and modeling motility of
644 Synechocystis sp. strain PCC6803. *J. Photochem. Photobiol. B* **91**, 77–86 (2008).

645 34. J.-S. Choi, *et al.*, Photomovement of the gliding Cyanobacterium Synechocystis sp. PCC
646 6803. *Photochem. Photobiol.* **70**, 95–102 (1999).

647 35. R. C. Hunter, T. J. Beveridge, High-resolution visualization of Pseudomonas aeruginosa
648 PAO1 biofilms by freeze-substitution transmission electron microscopy. *J. Bacteriol.* **187**,
649 7619–7630 (2005).

650 36. B. K. Pierson, R. W. Castenholz, Bacteriochlorophylls in gliding filamentous prokaryotes
651 from hot springs. *Nat. New Biol.* **233**, 25–27 (1971).

652 37. S. Hanada, A. Hiraishi, K. Shimada, K. Matsuura, Chloroflexus aggregans sp. nov., a
653 filamentous phototrophic bacterium which forms dense cell aggregates by active gliding
654 movement. *Int. J. Syst. Bacteriol.* **45**, 676–681 (1995).

655 38. S. Hanada, K. Shimada, K. Matsuura, Active and energy-dependent rapid formation of cell
656 aggregates in the thermophilic photosynthetic bacterium Chloroflexus aggregans. *FEMS*
657 *Microbiol. Lett.* **208**, 275–279 (2002).

658 39. L. Cai, *et al.*, Tad pilus-mediated twitching motility is essential for DNA uptake and survival
659 of Liberibacters. *PLoS One* **16**, e0258583 (2021).

660 40. S. Yoshihara, *et al.*, Mutational analysis of genes involved in pilus structure, motility and
661 transformation competency in the unicellular motile cyanobacterium Synechocystis sp. PCC
662 6803. *Plant Cell Physiol.* **42**, 63–73 (2001).

663 41. Y. Yang, *et al.*, Phototaxis in a wild isolate of the cyanobacterium Synechococcus
664 elongatus. *Proc. Natl. Acad. Sci. U. S. A.* **115**, E12378–E12387 (2018).

665 42. R. Allen, B. E. Rittmann, R. Curtiss 3rd, Axenic Biofilm Formation and Aggregation by
666 Synechocystis sp. Strain PCC 6803 Are Induced by Changes in Nutrient Concentration and
667 Require Cell Surface Structures. *Appl. Environ. Microbiol.* **85** (2019).

668 43. M. D. M. Aguilo-Ferretjans, *et al.*, Pili allow dominant marine cyanobacteria to avoid sinking
669 and evade predation. *Nat. Commun.* **12**, 1857 (2021).

670 44. D. Schatz, *et al.*, Self-suppression of biofilm formation in the cyanobacterium
671 Synechococcus elongatus. *Environ. Microbiol.* **15**, 1786–1794 (2013).

672 45. N. C. Caiazza, R. M. Q. Shanks, G. A. O'Toole, Rhamnolipids modulate swarming motility
673 patterns of Pseudomonas aeruginosa. *J. Bacteriol.* **187**, 7351–7361 (2005).

674 46. T. Ursell, R. M. W. Chau, S. Wisen, D. Bhaya, K. C. Huang, Motility enhancement through
675 surface modification is sufficient for cyanobacterial community organization during
676 phototaxis. *PLoS Comput. Biol.* **9**, e1003205 (2013).

677 47. N. Luo, S. Wang, J. Lu, X. Ouyang, L. You, Collective colony growth is optimized by
678 branching pattern formation in Pseudomonas aeruginosa. *Mol. Syst. Biol.* **17**, e10089

(2021).

48. B. R. Wucher, J. B. Winans, M. Elsayed, D. E. Kadouri, C. D. Nadell, Breakdown of clonal cooperative architecture in multispecies biofilms and the spatial ecology of predation. *Proc. Natl. Acad. Sci. U. S. A.* **120**, e2212650120 (2023).

49. J. B. Winans, B. R. Wucher, C. D. Nadell, Multispecies biofilm architecture determines bacterial exposure to phages. *PLoS Biol.* **20**, e3001913 (2022).

50. D. Nishiguchi, K. H. Nagai, H. Chaté, M. Sano, Long-range nematic order and anomalous fluctuations in suspensions of swimming filamentous bacteria. *Phys Rev E* **95**, 020601 (2017).

51. C. Tamulonis, J. Kaandorp, A model of filamentous cyanobacteria leading to reticulate pattern formation. *Life* **4**, 433–456 (2014).

52. H. Jeckel, *et al.*, Multispecies phase diagram of biofilm architectures reveals biophysical principles of biofilm development. *bioRxiv* 2021.08.06.455416 (2022).

53. T. Xu, *et al.*, Characterization of Mixed-Species Biofilms Formed by Four Gut Microbiota. *Microorganisms* **10** (2022).

54. D. Ren, J. S. Madsen, S. J. Sørensen, M. Burmølle, High prevalence of biofilm synergy among bacterial soil isolates in cocultures indicates bacterial interspecific cooperation. *ISME J.* **9**, 81–89 (2015).

55. L. L. Wong, *et al.*, Surface-layer protein is a public-good matrix exopolymer for microbial community organisation in environmental anammox biofilms. *ISME J.* **17**, 803–812 (2023).

56. Y.-M. Kim, *et al.*, Diel metabolomics analysis of a hot spring chlorophototrophic microbial mat leads to new hypotheses of community member metabolisms. *Front. Microbiol.* **6**, 209 (2015).

57. J. Z. Lee, *et al.*, Fermentation couples Chloroflexi and sulfate-reducing bacteria to Cyanobacteria in hypersaline microbial mats. *Front. Microbiol.* **5**, 61 (2014).

58. S.-I. Fukushima, “Analysis of gliding motility of the filamentous bacterium Chloroflexus aggregans.”

59. S. M. Boomer, K. L. Noll, G. G. Geesey, B. E. Dutton, Formation of multilayered photosynthetic biofilms in an alkaline thermal spring in Yellowstone National Park, Wyoming. *Appl. Environ. Microbiol.* **75**, 2464–2475 (2009).

60. B. M. Bebout, F. Garcia-Pichel, UV B-Induced Vertical Migrations of Cyanobacteria in a Microbial Mat. *Appl. Environ. Microbiol.* **61**, 4215–4222 (1995).

61. X. Zhang, B. Ji, J. Tian, Y. Liu, Development, performance and microbial community analysis of a continuous-flow microalgal-bacterial biofilm photoreactor for municipal wastewater treatment. *J. Environ. Manage.* **338**, 117770 (2023).

62. M. Nierychlo, *et al.*, The morphology and metabolic potential of the Chloroflexi in full-scale activated sludge wastewater treatment plants. *FEMS Microbiol. Ecol.* **95** (2019).

63. A. Sood, N. Renuka, R. Prasanna, A. S. Ahluwalia, “Cyanobacteria as Potential Options for Wastewater Treatment” in *Phytoremediation: Management of Environmental Contaminants, Volume 2*, A. A. Ansari, S. S. Gill, R. Gill, G. R. Lanza, L. Newman, Eds. (Springer International Publishing, 2015), pp. 83–93.

64. D. Brockmann, *et al.*, Wastewater treatment using oxygenic photogranule-based process has lower environmental impact than conventional activated sludge process. *Bioresour. Technol.* **319**, 124204 (2021).

65. M. Nierychlo, *et al.*, Candidatus Amarolinea and Candidatus Microthrix Are Mainly Responsible for Filamentous Bulking in Danish Municipal Wastewater Treatment Plants. *Front. Microbiol.* **11**, 1214 (2020).

66. K. Heimann, Novel approaches to microalgal and cyanobacterial cultivation for bioenergy and biofuel production. *Curr. Opin. Biotechnol.* **38**, 183–189 (2016).

67. M. Bozan, A. Schmid, K. Bühler, Evaluation of self-sustaining cyanobacterial biofilms for technical applications. *Biofilms* **4**, 100073 (2022).

68. R. W. Castenholz, “Isolation and Cultivation of Thermophilic Cyanobacteria” in *The Prokaryotes: A Handbook on Habitats, Isolation, and Identification of Bacteria*, M. P. Starr, H. Stolp, H. G. Trüper, A. Balows, H. G. Schlegel, Eds. (Springer Berlin Heidelberg, 1981), pp. 236–246.

69. S. Hanada, A. Hiraishi, K. Shimada, K. Matsuura, Isolation of *Chloroflexus aurantiacus* and related thermophilic phototrophic bacteria from Japanese hot springs using an improved isolation procedure. *J. Gen. Appl. Microbiol.* **41**, 119–130 (1995).

70. J. Schindelin, *et al.*, Fiji: an open-source platform for biological-image analysis. *Nat. Methods* **9**, 676–682 (2012).

71. D. Ershov, *et al.*, TrackMate 7: integrating state-of-the-art segmentation algorithms into tracking pipelines. *Nat. Methods* **19**, 829–832 (2022).

72. R Core Team, R: A Language and Environment for Statistical Computing. [Preprint] (2024). Available at: https://www.R-project.org/.

73. P. A. Zaini, L. De La Fuente, H. C. Hoch, T. J. Burr, Grapevine xylem sap enhances biofilm development by Xylella fastidiosa. *FEMS Microbiol. Lett.* **295**, 129–134 (2009).

74. M. Román-Écija, *et al.*, Two Xylella fastidiosa subsp. multiplex Strains Isolated from Almond in Spain Differ in Plasmid Content and Virulence Traits. *Phytopathology* **113**, 960–974 (2023).

75. J. R. Kremer, D. N. Mastronarde, J. R. McIntosh, Computer visualization of three-dimensional image data using IMOD. *J. Struct. Biol.* **116**, 71–76 (1996).

## Supplementary methods

### Plasmid construction for *ΔpilB* knockout in Syn OS-B'

A construct containing a thermostable kanamycin resistance cassette ($Km_{Te}^{R}$), flanked by up- and down-stream regions homologous to the *pilB* (CYB_2143) deletion site was built in pGEM®-T easy (Promega). The pT7BT/P cpcC::KmTe plasmid containing the thermostable kanamycin resistance cassette from *Thermosynechococcus elongatus* ($Km_{Te}^{R}$) was a generous gift from Kiyoshi Onai (Nagoya University) (1). The fragments were amplified by PCR with primers 1-3 (Table S1) using Phusion High Fidelity PCR Kit (New England Biolabs, USA) and assembled with NEBuilder® HiFi DNA Assembly Master Mix (USA). The construct was cloned in *E. coli* DH5-α and confirmed by Sanger sequencing through ELIM biopharmaceuticals Inc. (USA). In OS-B', the *pilB* gene may be included in an operon that includes putative pilus-related genes *pilT* and *pilC* downstream of *pilB*. To avoid a potential polar effect by the disruption of the *pilB* gene, several factors were considered as outlined in (2): i) the KanR was inserted in the same orientation as the genes in the putative operon, ii) no transcriptional terminator in the KanR was included, iii) the KanR was inserted by the 3' end of the gene but maintaining at least a few codons of the 3' end of the ORF (101 bp), and iv) the size of the deletion (1,210 bp) is similar to the insertion (878 bp).

### Transformation of Syn OS-B'

Syn OS-B' cells were grown under continuous light at 50°C on DH10 medium supplemented with 250 mg/l of bacto-tryptone (DH10+BT) (3) until late log phase (OD600nm~0.6). Cells were adjusted to OD730nm = 60 in 80 µl and incubated with 20 ng/µl of pDNA overnight for natural transformation (1). After incubation, the cells were spread onto two-layer DH10+BT tight-fit bacteriological plates (1% and 0.4% agarose bottom and top layers), and incubated at 50°C under continuous light. After 8-10 days, a kanamycin concentration gradient was created by lifting the bottom agarose layer and adding 40 µL of 30 µg/ml of kanamycin. After 6-8 weeks, antibiotic-resistant colonies were picked and segregated in DH10+BT liquid medium with increasing concentrations of antibiotic to reach homoplasmy, transferring to fresh medium weekly for 3 weeks. The clones were genotyped by PCR using primers 12-14, which bind up and downstream of the homology regions used for recombination, and confirmed by Sanger sequencing. RT-qPCR using primers 4-11 (Table S1) on RNA from Syn OS-B' and *ΔpilB* cells grown to late-log phase in DH10 medium indicated that there was no obvious polar effect on *pilC*, which is downstream of *pilB*, since it was expressed at similar levels in Syn OS-B' and *ΔpilB* (Figure S4). Six clones were confirmed and used for motility assays.

### RT-qPCR

Syn OS-B' and *ΔpilB* were grown in 15 ml of DH10 medium until late log phase (OD600nm~0.6). Flasks were swirled in liquid nitrogen to chill cultures to <4℃ in <30 seconds, transferred to prechilled 15 ml tubes, centrifuged at 4,000 *g* for 5 minutes, supernatant discarded, and loose pellet transferred to a 1.5 ml tube for a 2-minute 4,000 *g* centrifugation, supernatant removal, and snap-freezing in liquid nitrogen. RNA was extracted using a Quick-

RNA kit (Zymo Cat#R2014) according to the manufacturer's instructions, with an additional DNAse digestion step with an RNAse-free DNAse set (Qiagen Cat#79254) according to the manufacturer's instructions. 400 ng of RNA was reverse-transcribed to cDNA using the iScript Reverse Transcription Supermix (Bio-Rad Cat#1708841). cDNA was diluted 10-fold and 4 µL was added to a master mix of 5µL 2× SensiFAST SYBR No-ROX kit reaction mix (Meridian Bioscience Cat#98050) plus 0.5 µL of each 10 mM primer stock (Table S1). PCR amplification was performed over 45 cycles of 95°C for 10 s and 60°C for 30 s with fluorescence quantification at the end of each cycle, followed by melting curve analysis by ramping the temperature from 65°C to 97°C at 0.11°C per second. Absence of gDNA contamination was confirmed by also supplying no-reverse transcriptase cDNA synthesis controls as qPCR templates and finding threshold cycle values >40. qPCR target specificity was confirmed by a single peak in the melt profile with a melt temperature <2℃ from the median for that target. The mean threshold cycle of 4 genes (cysE, La, U32, SufS) served as the housekeeping controls and relative transcript abundances calculated according to the ΔCt method ($2^{-(\text{Ct target gene} - \text{Ct HK mean})}$).

## References


1. K. Onai, M. Morishita, T. Kaneko, S. Tabata, M. Ishiura, Natural transformation of the thermophilic cyanobacterium Thermosynechococcus elongatus BP-1: a simple and efficient method for gene transfer. *Mol. Genet. Genomics* **271**, 50–59 (2004).

2. L. P. Sáez, *et al.*, Cyanate Assimilation by the Alkaliphilic Cyanide-Degrading Bacterium Pseudomonas pseudoalcaligenes CECT5344: Mutational Analysis of the cyn Gene Cluster. *Int. J. Mol. Sci.* **20** (2019).

3. F. Bunbury, *et al.*, Differential Phototactic Behavior of Closely Related Cyanobacterial Isolates from Yellowstone Hot Spring Biofilms. *Appl. Environ. Microbiol.* **88**, e0019622 (2022).

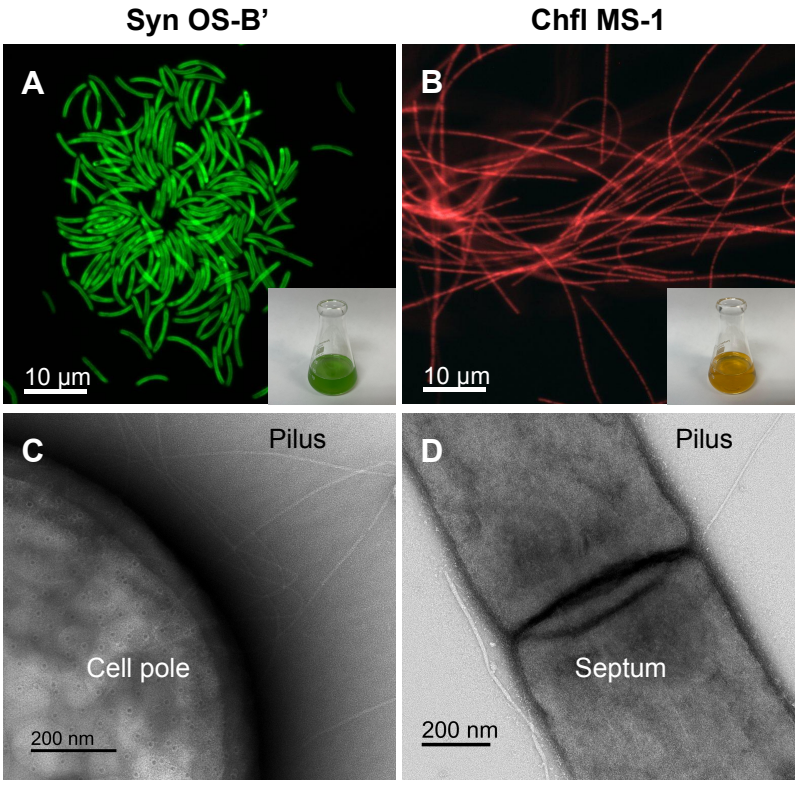


**Figure S1. Hot spring isolates Syn OS-B' and Chfl MS-1 are pigmented and piliated. (A)** Fluorescence micrograph of Syn OS-B' (ex. 540-580 nm / em. 608-682 nm); inset: culture of Syn OS-B' in DH10M medium. **(B)** Fluorescence micrograph of Chfl MS-1 (ex.450-490 nm / em. >515 nm); inset: culture of Chfl MS-1 in PE medium. **(C)** TEM image of uranyl-acetate-stained cell pole of Syn OS-B' exhibiting T4P (8 nm diameter). (**D**) TEM image of Chfl MS-1 showing the septum between adjacent cells in a filament and a pilus (7 nm diameter) emerging from near the septum.

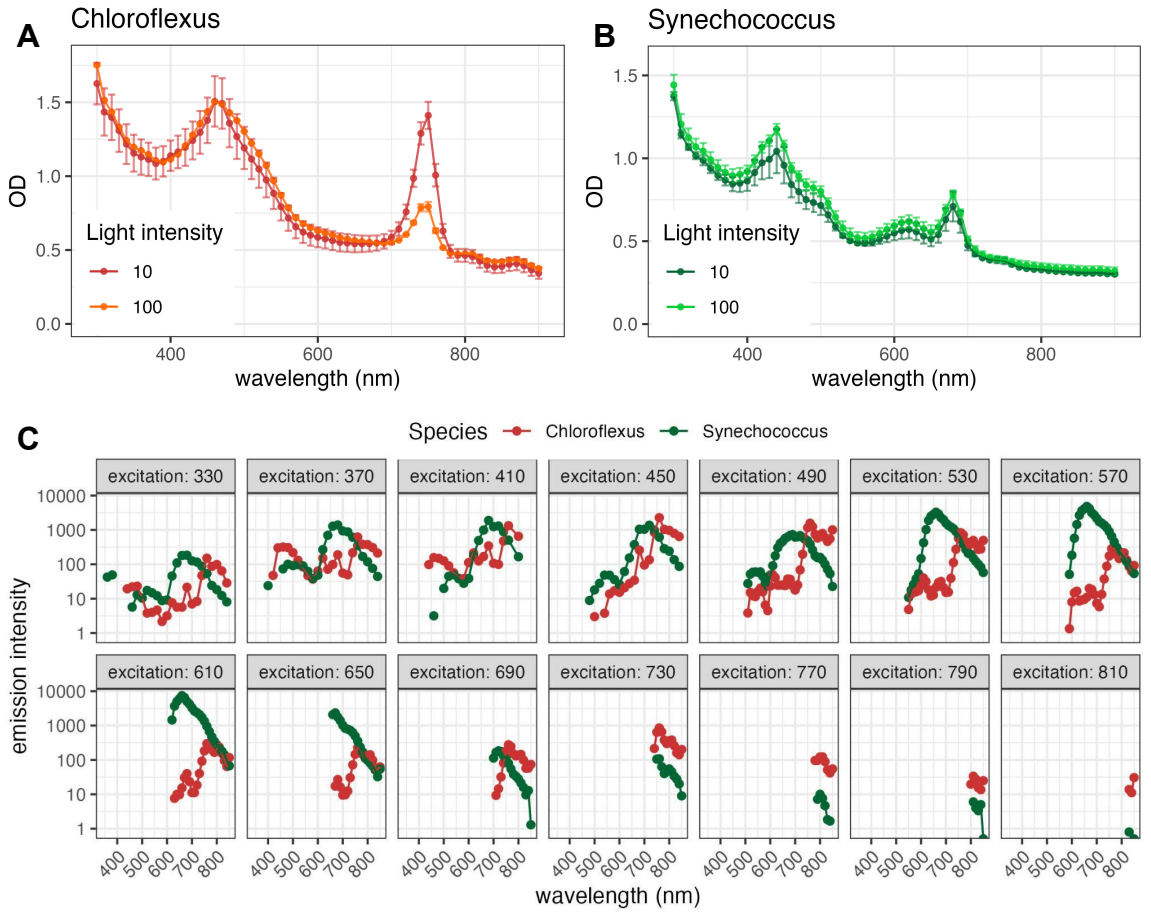


**Figure S2. Absorption and fluorescence emission spectra of Chloroflexus (Chfl MS-1) and Synechococcus (Syn OS-B') cultures. (A)&(B)** Absorption spectra of Syn OS-B' and Chfl MS-1 grown at 10 or 100 $\mu mol \cdot m^{-2} \cdot s^{-1}$ in dark and light colours respectively. **(C)** Fluorescence emission spectra of Chfl MS-1 (orange) and Syn OS-B' (green) after excitation at different wavelengths indicated above each panel. Points represent means, error bars represent SD, n=3.

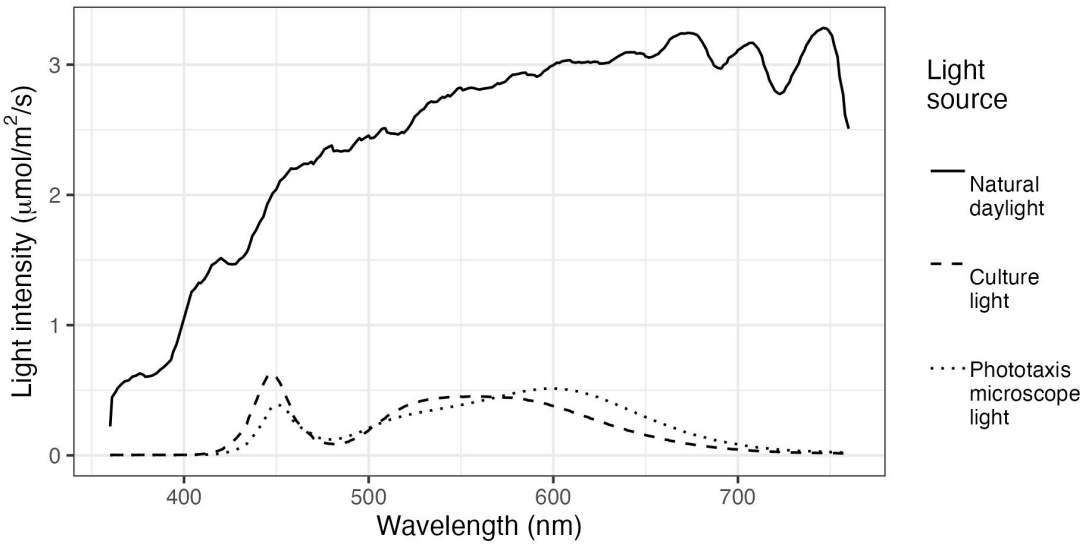


**Figure S3. Light spectra of different light sources.** Light spectra were measured with a Hipoint spectrophotometer between 360 and 760 nm. Natural daylight was recorded vertically at 3pm on the 03/25/21 (a partly sunny day) at 37°25'42.8"N 122°10'47.0"W. Culture light: spectrum during preculturing and collective motility assays (measured at the nearest edge of the culture vessels). Phototaxis microscope light: spectrum when measuring single cell phototactic/motility responses in a temperature-controlled microscope at the same point as the cells.

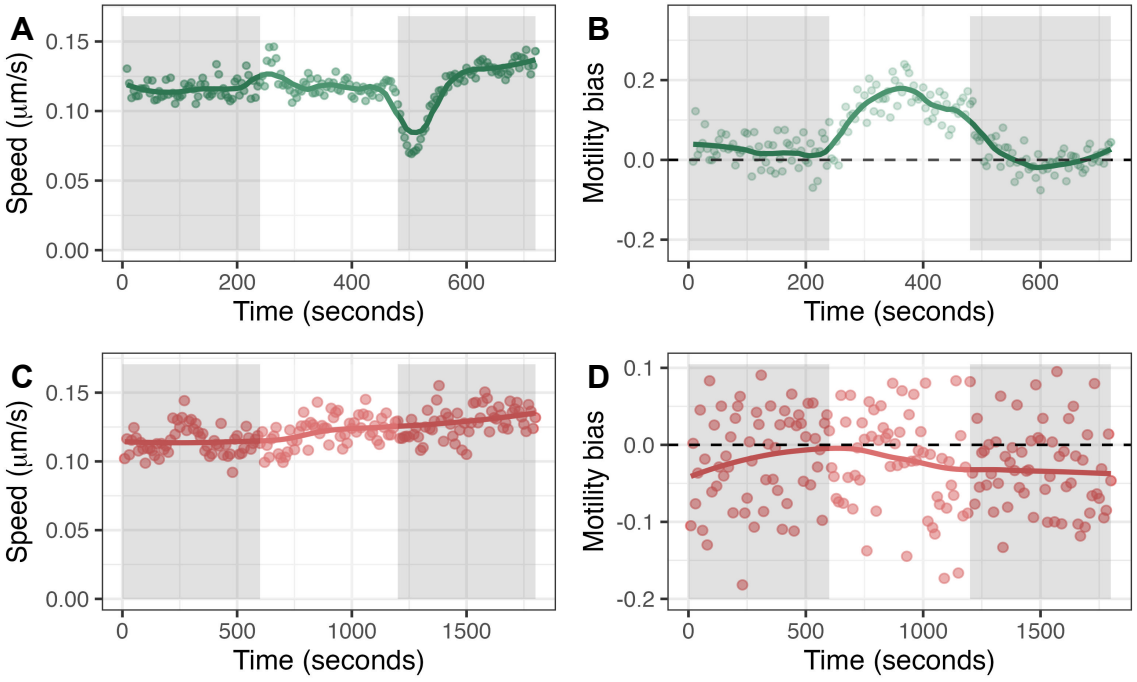


**Figure S4. Syn OS-B' cells and Chfl MS-1 filaments move differently during light transitions.** Syn OS-B' and Chfl MS-1 were both plated on DH10 solidified with 0.4% agarose, but Syn OS-B' was incubated under directional white light for 2-4 days prior to tracking cells within phototactic projections, while Chfl MS-1 was incubated for 2-6 hours and filament tips tracked from within the starting droplet area. Cells were incubated in the microscope in the dark for >5 minutes then recorded under 4 or 10 minute periods (Syn OS-B' and Chfl MS-1, respectively) of darkness, then 50 $\mu mol \cdot m^{-2} \cdot s^{-1}$ white light from right, then darkness. Chfl MS-1 filaments were tracked with a custom tip-tracking algorithm (see methods) and Syn OS-B' cells by ImageJ using the Weka trainable segmentation and Trackmate plugins. Note that data in panels A&B are also shown in Figure 3 H&I. **(A)** Speed of tracked Syn OS-B' cells within phototactic projections during light transitions. **(B)** Motility bias (proportion of movement towards light. 0 = random) of tracked Syn OS-B' cells within phototactic projections during light transitions. **(C)** Speed of tracked Chfl MS-1 filaments. **(D)** Motility bias of Chfl MS-1 filaments. Each point represents the mean of >100 Chfl MS-1 tips or >300 Syn OS-B' cells from 8-10 separate videos.

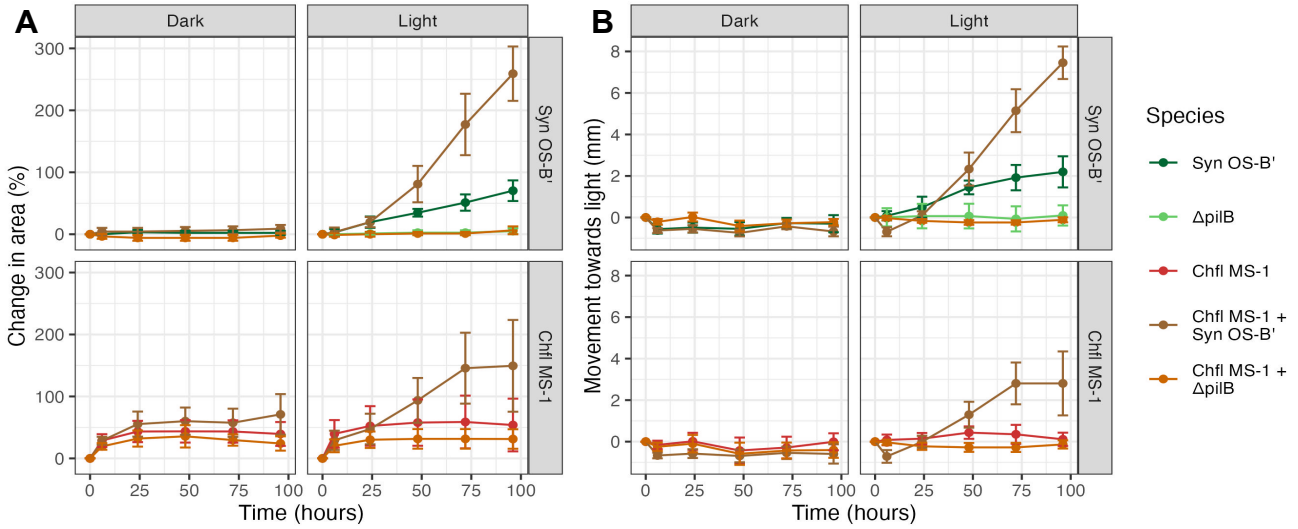


**Figure S5. Syn OS-B'-Chfl MS-1 interactions improve movement towards the light. (A)** Change in area of colonies. **(B)** Movement towards the light source of species mixtures. Syn OS-B' chlorophyll signal (top panels) and Chfl MS-1 bacteriochlorophyll signal (bottom panels) in the dark (left panels) and directional 50 $\mu mol \cdot m^{-2} \cdot s^{-1}$ white light (right panel), with different species mixtures indicated by colours listed in the legend to the right. N=12 biological replicates from 2 experiments, and error bars indicate 95% confidence interval of the mean.

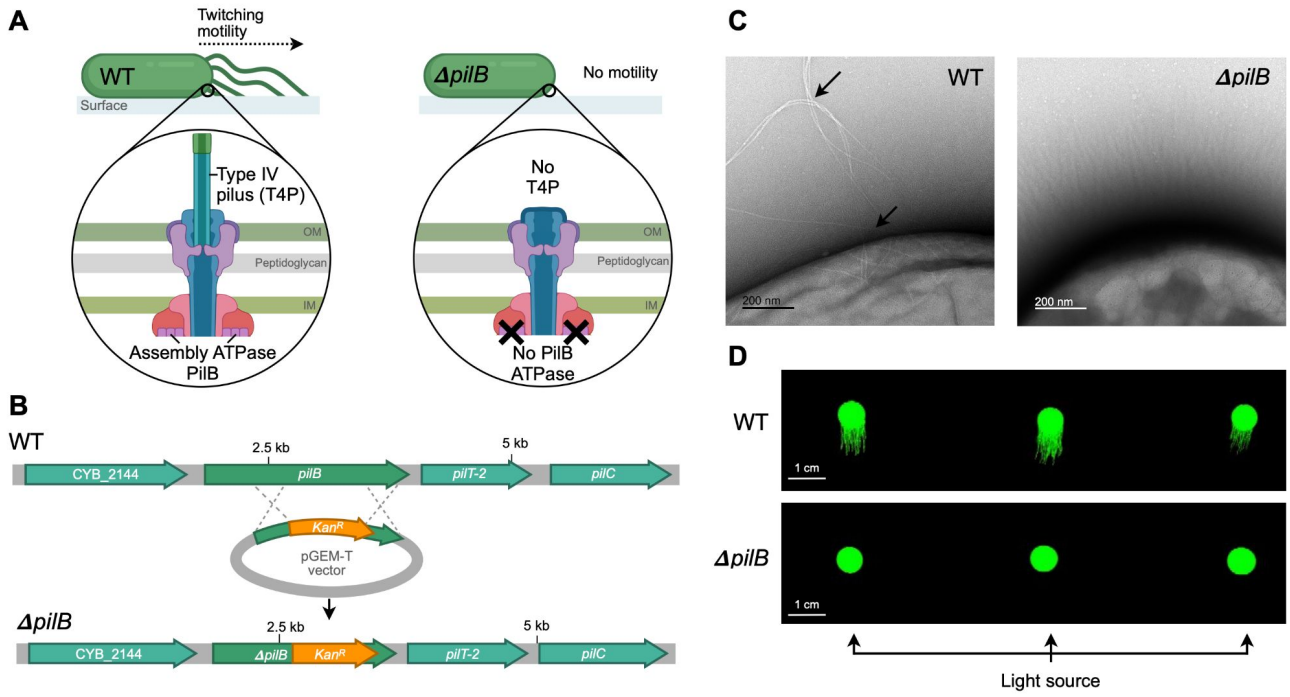


**Figure S6. Syn OS-B' *ΔpilB* mutants lack Type IV pili and motility. (A)** Schematic of the intended effect of knocking out pilB in Syn OS-B': the cells become non motile due to the lack of T4P, which is due to an inability to assemble pilin subunits into a pilus. OM, outer membrane; IM, inner membrane. **(B)** Diagram of the protocol by which a plasmid containing a Kanamycin resistance cassette (KanR) flanked by *pilB* sequences allowed integration into the *pilB* gene by homologous recombination using natural transformation of Syn OS-B'. **(C)** Transmission electron microscopy of Syn OS-B' (WT (left) and *ΔpilB* (right)) shows T4P pili only in WT (indicated by black arrows), and regions of either EPS or thin pili in both (indicated by white arrows). Additional images are provided in Figures S5 and S6. **(D)** Chlorophyll fluorescence scans of 3 representative replicates of Syn OS-B' cells (top) and independent *ΔpilB* knockouts (bottom) incubated under directional (from bottom) white light for 4 days, showing phototaxis of Syn OS-B' but not *ΔpilB*, towards the light. Image in A created with BioRender.com.

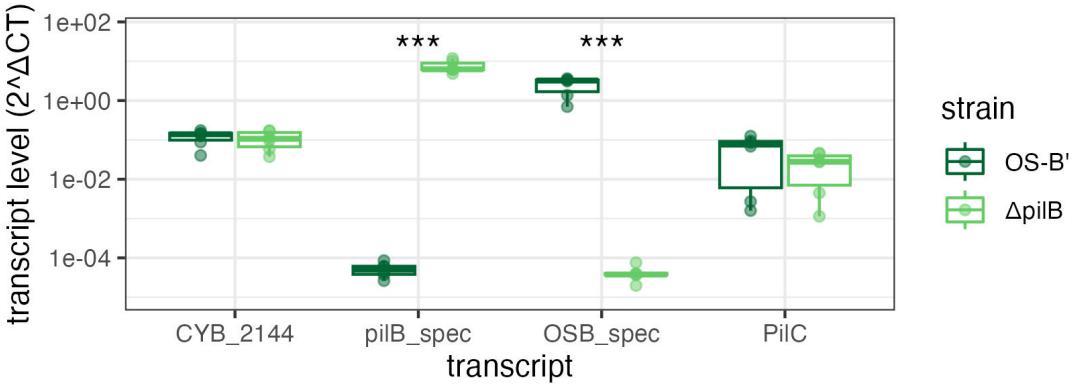


**Figure S7. RT-qPCR on Syn OS-B' and *ΔpilB* mutants reveals complete knockout of *pilB* gene and maintained expression of other genes in the operon.** RNA was extracted from six late log-phase cultures of Syn OS-B' and from six independent *ΔpilB* mutant cultures, reverse transcribed, and cDNA was quantified by qPCR. Primers were designed to amplify <300bp regions from the gene 5' to *pilB* (CYB_2144), the kanamycin resistance cassette found only in *ΔpilB* (pilB_spec), the region of *pilB* that was knocked out and therefore only present in Syn OS-B' (OSB_spec), and *pilC*, which is 3' to *pilB* and possibly in the same operon. Transcript concentration is displayed on the y-axis and calculated by raising 2 to the power of the the threshold cycle value of the target gene subtracted from the mean threshold cycle of four housekeeping genes (cysE, La, U32, SufS) ($2^{-\Delta CT}$ method). Student's t-tests were performed with Bonferroni correction with statistical significance reported as follows: *** = $p<0.001$, otherwise $p>0.05$.

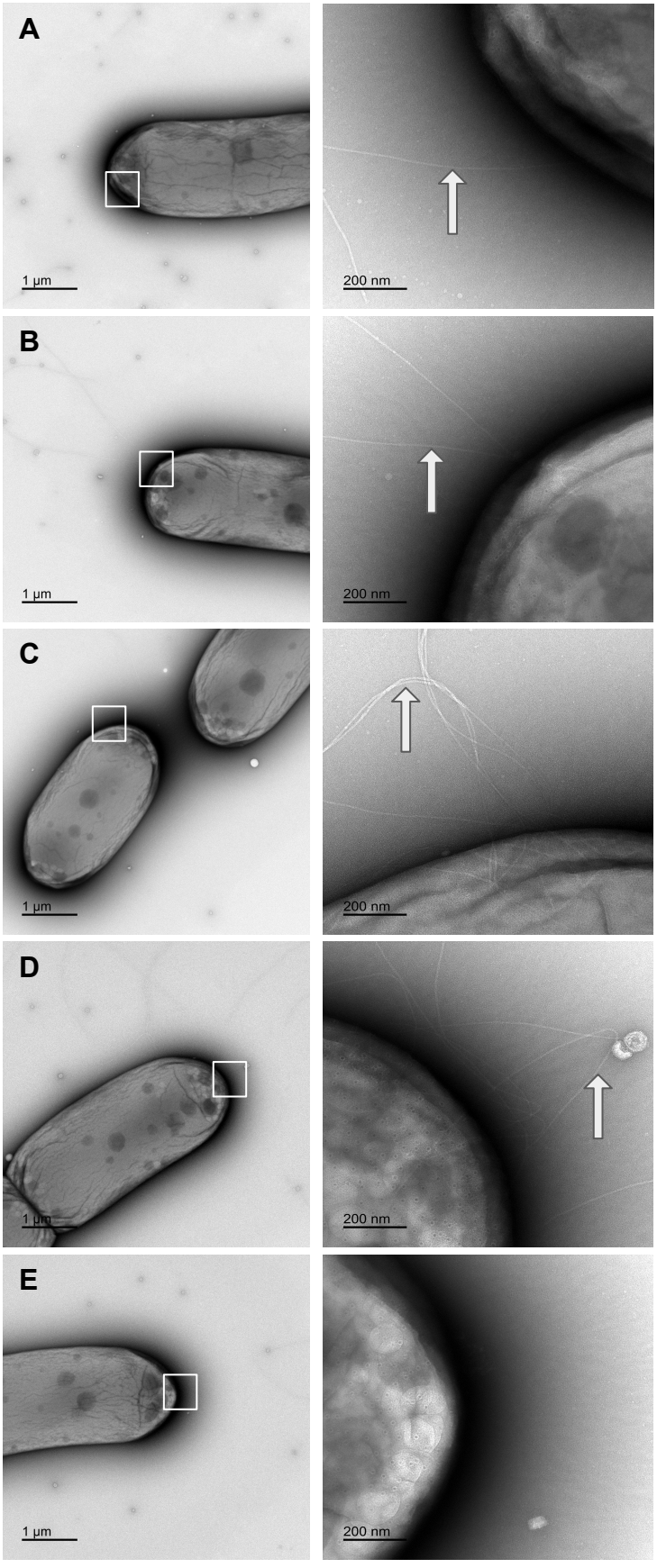


**Figure S8. Transmission electron microscopy of Syn OS-B' cells reveals thick pili (indicated by arrows)**. Cells were stained with uranyl acetate and mounted on TEM grids prior to imaging. 5 cells were randomly selected and a magnified image of one of their poles was captured. 4 out of 5 cells had thick pili near their poles.

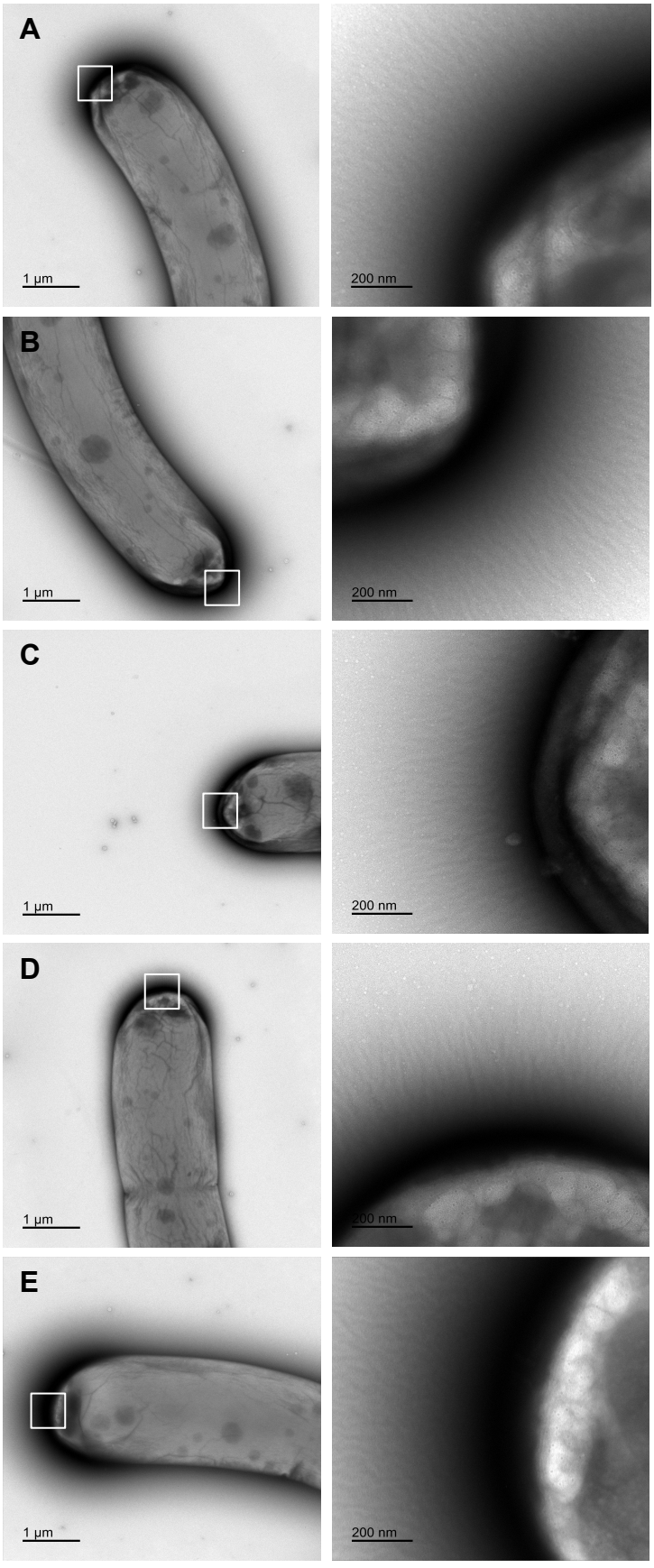


**Figure S9. Transmission electron microscopy of *ΔpilB* cells reveals absence of thick pili.** Cells were stained with uranyl acetate and mounted on TEM grids prior to imaging. Five cells were randomly selected and a magnified image of one of their poles was captured. 0 out of 5 cells had thick pili near their poles.

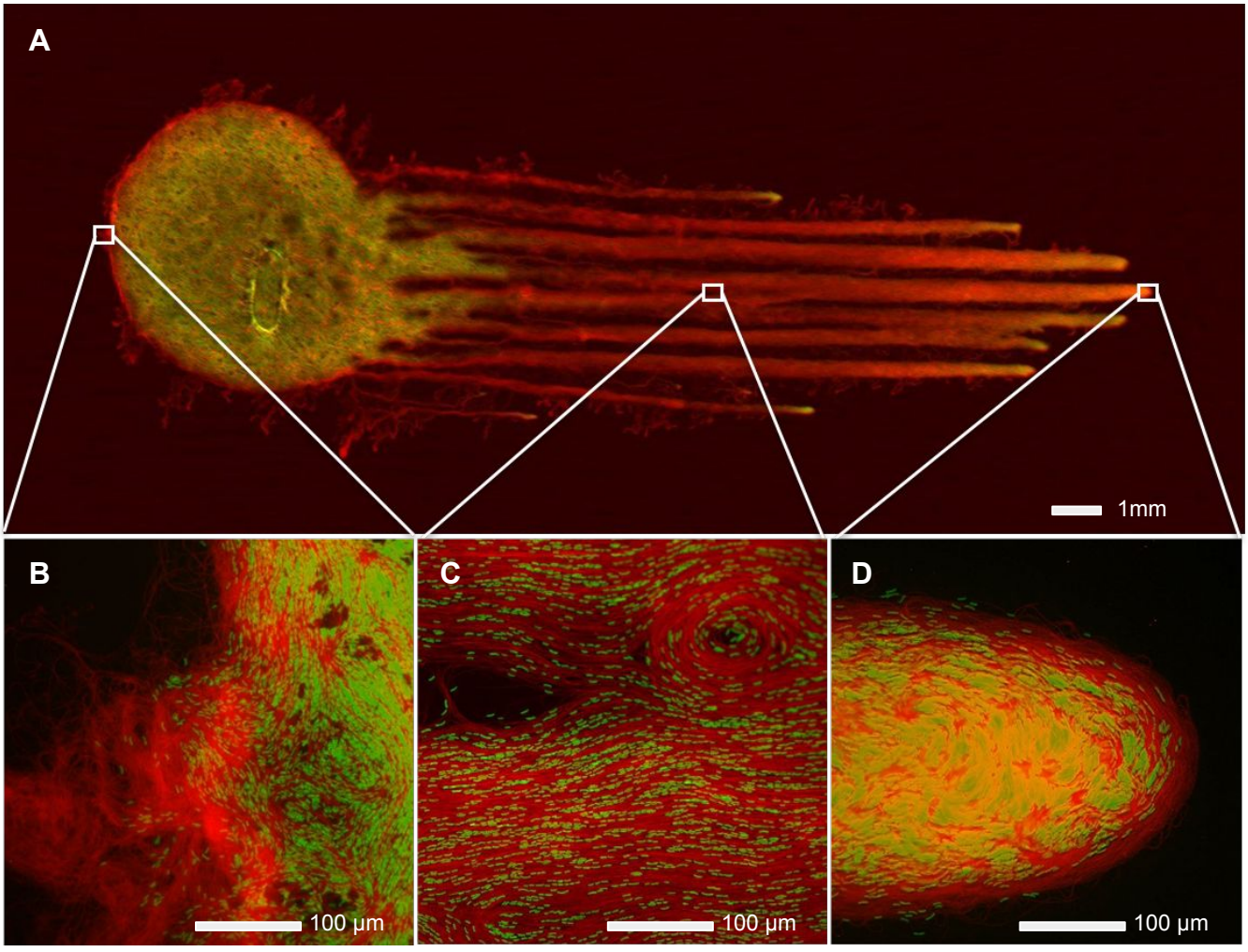


**Figure S10. Viewing Chfl MS-1-Syn OS-B' consortium motility with fluorescence scanning and microscopy.** Images were taken after 4 days incubation under directional (from right) 60 µmol·m$^{-2}$·s$^{-1}$ white light. **(A)** Fluorescence microscopy with excitation 784 nm and emission at 832 nm (band pass of 37 nm) (red) and by excitation 658 nm and emission at 710 nm (band pass of 40 nm) (green). **(B,C,D)** Fluorescence micrographs of Chfl MS-1 + Syn OS-B' from selected regions (squares) with excitation at 450-490 nm and emission at >515 nm (red), and excitation at 540-580 nm and emission at 608-682 nm (green).

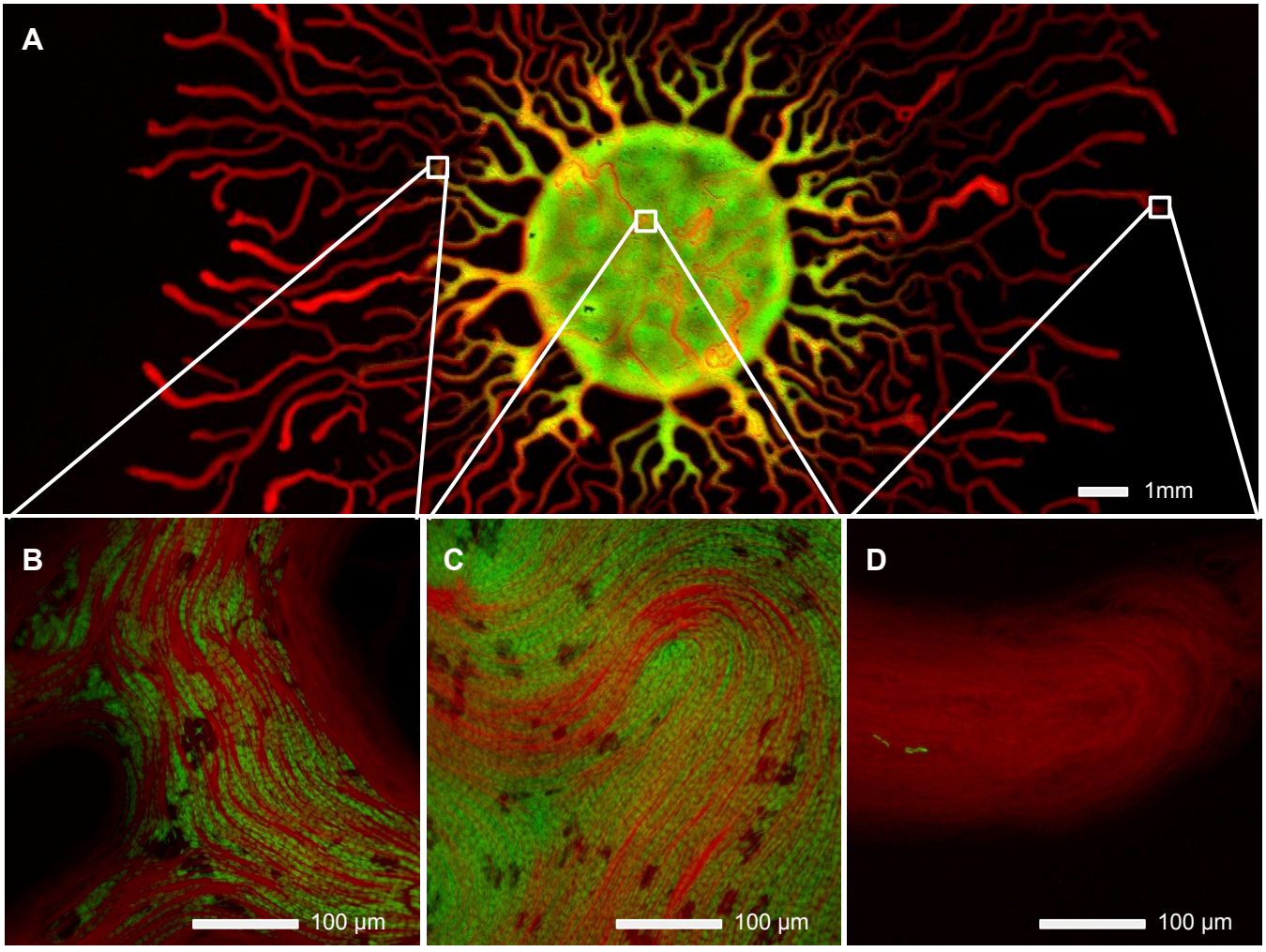


**Figure S11. Viewing Chfl MS-1-*ΔpilB* consortium motility with fluorescence scanning and microscopy.** Images were taken after 4 days incubation under directional (from right) 60 µmol·m$^{-2}$·s$^{-1}$ white light. **(A)** Fluorescence microscopy with excitation 784 nm and emission at 832 nm (band pass of 37 nm) (red) and by excitation 658 nm and emission at 710 nm (band pass of 40 nm) (green). **(B,C,D)** Fluorescence micrographs of Chfl MS-1 + *ΔpilB* from selected regions (squares) in panel A with excitation at 450-490 nm and emission at >515 nm (red), and excitation at 540-580 nm and emission at 608-682 nm (green).

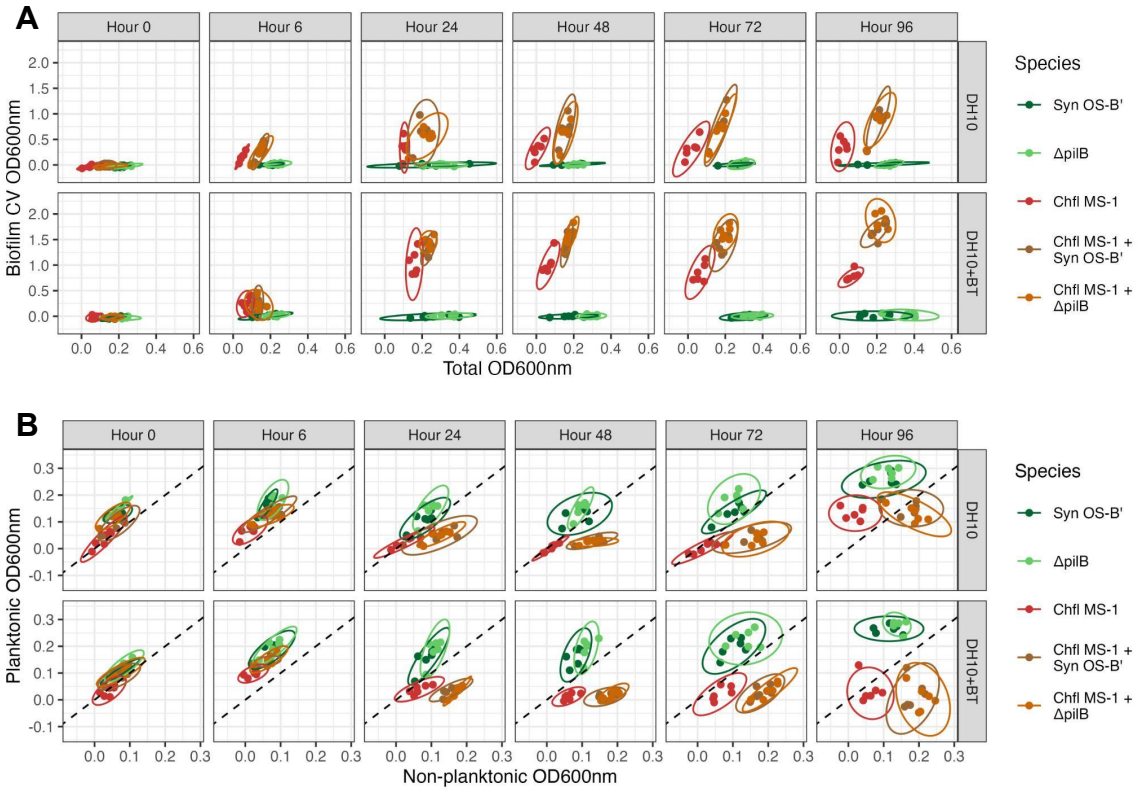


**Figure S12. Binary consortia consistently develop more biofilm and less planktonic cells than axenic cyanobacteria over time. (A)** After 0-4 days of incubation of cultures, OD600nm absorption measurements were taken on the total culture (x-axis) and after crystal violet staining of the biofilm (y-axis). **(B)** After 0-4 days, cultures were briefly disrupted by pipetting and 80% of the culture volume was transferred to a new plate. OD600nm was measured in the 20% of the remaining volume and called "Non-planktonic OD600nm" (x-axis), and in the transferred volume and called "Planktonic OD600nm" (y-axis). Top panel labels indicate the time of sampling after inoculation, side panel labels indicate culture medium (DH10 or DH10 + BT (bactotryptone). Colours represent the species in cultures, as indicated by the legend to the right, and ellipses indicate the 95% confidence intervals of the measurements. N=6 independent biological replicates for every timepoint and medium.

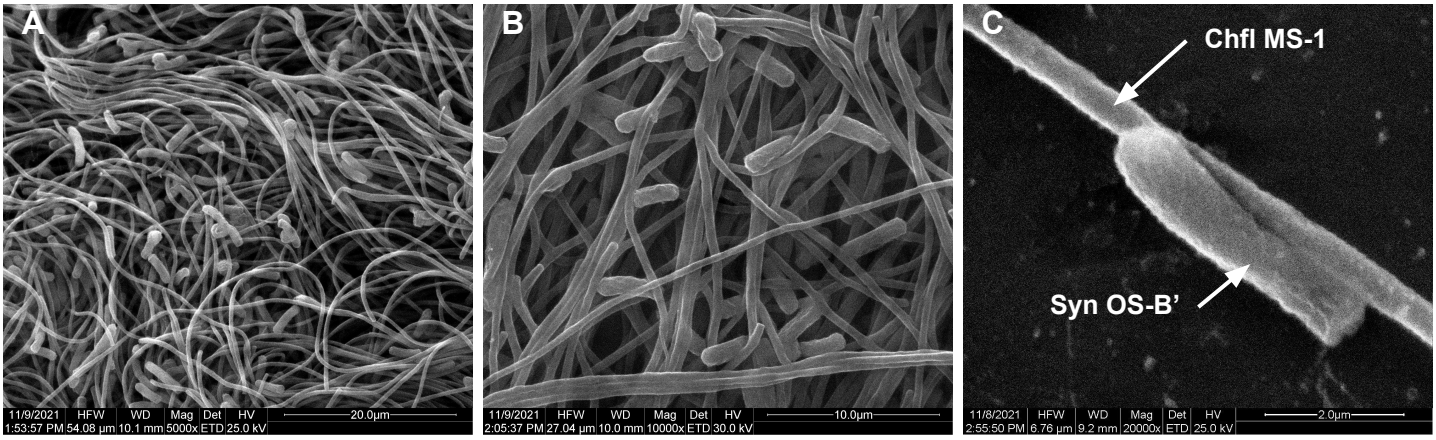


**Figure S13. Scanning electron microscopy of Syn OS-B' and Chfl MS-1 binary consortium reveals that the species are often associated with one another**. The samples were imaged in Quanta 200 (FEI) SEM with 25 kV accelerating voltage in high vacuum with secondary emission (SE) detector. Increasing magnification from left to right **(A)** 5000x, **(B)** 10,000x, **(C)** 20,000x.

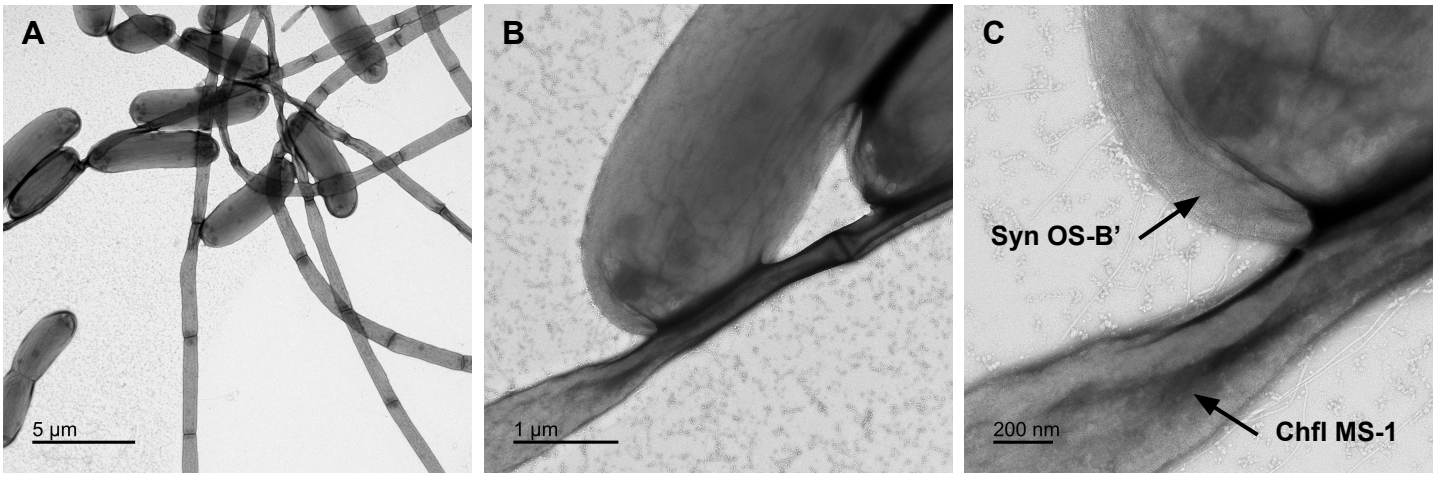


**Figure S14. Transmission electron microscopy of Syn OS-B' and Chfl MS-1 binary consortium reveals that the species are often associated with one another.** The grids with uranyl-acetate stained cells were imaged in JEOL JEM-1400 with 120 kV accelerating voltage equipped with a Gatan Inc. OneView 4kX4k sCMOS camera. Increasing magnification from left to right **(A)** 5,000x, **(B)** 30,000x, **(C)** 80,000x.

| Number | Purpose | Name | Forward primer (5'-3') | Reverse primer (5'-3') |
|---|---|---|---|---|
| 1 | Assembly | Up flank | ccatggcggccgcgggaattcgattAACGATCTTCCTCCCCCTC | gggcaacgaagggaaacgcctattaGACAGTTTAATAATCGGGGCATC |
| 2 | Assembly | $Kan_{Te}^{R}$ | TAATAGGCGTTTCCCTTC | CTAAAAGGGAATGCGTTTG |
| 3 | Assembly | Down flank | tgtgagcaaacgcattccctttagCTGAAGGCCCGTGCCAAG | aggcggccgcgaattcactagtgatCGGTAGACGTTCACGCGG |
| 4 | qPCR (Syn OS-B' only) | CYB_2143 (pilB) | CATCCGCTTCCGCAAAGATG | TGACCCGAAAGTCCACCTTG |
| 5 | qPCR (3' to *pilB*) | CYB_2141 (pilC) | TCCATCGACATTCGCGACAA | CCGGTTTGCTCCTCCATGAT |
| 6 | qPCR (5' to *pilB*) | CYB_2144 | GTGTGTCTCTCCACCTTGGG | GGCAAACATGGCCACCAAAT |
| 7 | qPCR (*ΔpilB* only) | kanR | CATCCGCTTCCGCAAAGATG | TGACCCGAAAGTCCACCTTG |
| 8 | qPCR (housekeeping) | CYB_0494 (La) | AGTACCGCTACCGCATGATG | GCAACACCTCAGCACAACAG |
| 9 | qPCR (housekeeping) | CYB_0970 (U32) | GGTTTACCGGGTGCAAGAGA | CGTGAACCTCCATGTGGACA |
| 10 | qPCR (housekeeping) | CYB_1997 (SufS) | ACAGGTAAACACTGGCTCGG | TAGCTTTTCGGTGGAGGCTG |
| 11 | qPCR (housekeeping) | CYB_2852 (cysE) | CTTCGCCTCTCACCTGATCC | TGGCATTGACCTGGATCACC |
| 12 | Genotyping | *ΔpilB-1* | GGCAGATGATGCCCCGATTA | AAAACTTCGGGGTCAGGCAA |
| 13 | Genotyping | *ΔpilB-2* | TCGTCAAGTTCGGCAATCCA | TTCCACTTGGCTGGCGTAAT |
| 14 | Genotyping | *ΔpilB-3* | ATTACGCCAGCCAAGTGGAA | TTGCTCCAGCGTTTTCATGC |

**Table S1. Primers used in this study.** Primers were used to create the construct used for transformation (Assembly), test whether *pilB* was replaced by the cassette in *ΔpilB* (Genotyping), and to test for a polar effect of the kanamycin resistance cassette insertion by quantifying relative transcript levels of nearby genes (qPCR).